OFDM Communications over Time-Varying Channels

7

Luca Rugini[1], Paolo Banelli[1], Geert Leus[2]

[1]*University of Perugia, Perugia, Italy*
[2]*Delft University of Technology, Delft, The Netherlands*

7.1 OFDM SYSTEMS

Orthogonal frequency-division multiplexing (OFDM), also known as multicarrier modulation (Bingham, 1990; Cimini Jr, 1985; Keller & Hanzo, 2000; Le Floch, Alard, & Berrou, 1995; Sari, Karam, & Jeanclaude, 1995; Wang & Giannakis, 2000; Zou & Wu, 1995), relies on the concept of parallel data transmission in the frequency domain and mainly owes its success to the easy equalization for linear time-invariant (LTI) frequency-selective channels. In OFDM systems, the data symbol stream is split into L parallel flows, which are transmitted on equispaced frequencies called subcarriers, each one characterized by a transmission rate that is $1/L$ times lower than the original data rate. This is obtained by splitting the original data stream into multiple blocks, which are transmitted in consecutive time intervals, where each symbol of a block is associated to a specific subcarrier. This frequency-domain multiplexing can be efficiently performed by means of fast Fourier transform algorithms.

Due to the use of orthogonal (equispaced) subcarriers, OFDM systems with LTI frequency-selective channels avoid the so-called intercarrier interference (ICI) among the data symbols of the same OFDM block. Differently from conventional frequency-division multiplexing, a frequency overlapping among the spectra associated to different substreams is permitted, resulting in a significant reduction of the bandwidth requirements. Moreover, for LTI frequency-selective channels, the absence of ICI allows an easy channel equalization, which can be performed on a per-subcarrier basis by means of scalar divisions. The *intersymbol interference* (ISI)[1] among data symbols of different OFDM blocks, induced by multipath propagation, is avoided by a suitable cyclic extension of each OFDM block, usually referred to as *cyclic prefix* (CP) (Sari et al., 1995; Wang & Giannakis, 2000; Zou & Wu, 1995).

However, when the channel experiences a nonnegligible time variation, each subcarrier undergoes a Doppler spreading effect that destroys the subcarrier orthogonality, producing significant ICI (Robertson & Kaiser, 1999; Russell & Stüber, 1995; Stantchev & Fettweis, 2000). Dually to the ISI in single-carrier systems, the ICI power reduces the *signal-to-interference-plus-noise ratio* (SINR) and, when left uncompensated, impairs the performance of OFDM systems. A simple method that reduces the ICI is the shortening of the OFDM block duration. This way the channel becomes (almost) constant

---

[1]The ISI is also known as *interblock interference*, while the OFDM blocks are also known as *OFDM symbols*.

over each block. However, the block-length shortening is capacity inefficient, because the CP has to be inserted more frequently. Therefore, other ICI mitigation techniques are necessary. These techniques are reviewed in Section 7.2. In addition, the rapid time variation of the channel makes its estimation more complicated. This issue is discussed in Section 7.3.

In this section, we first set up the system model and review the behavior of OFDM systems with LTI channels, focusing on the most popular OFDM wireless standards. Subsequently, we show the effects of rapidly time-varying channels on conventional OFDM systems by analyzing the ICI power, the SINR degradation, and the bit-error rate (BER) performance loss. Finally, we extend the system model to multiantenna OFDM systems.

7.1.1 System Model

We consider an OFDM system with L equispaced subcarriers, where F is the subcarrier separation and L_{CP} is the size of the CP that is prepended to each OFDM block. The whole OFDM system we are going to describe is depicted in Fig. 7.1.

After serial-to-parallel conversion, the stream of symbols is split into data blocks. Each OFDM block, of size L, can contain either data symbols or pilot symbols, or both data and pilots, depending on the training pattern. The pilot symbols may be used at the receiver side for time and frequency synchronization, channel estimation, phase offset correction, and so on. Virtual carriers, which are included in every OFDM system as guard bands to prevent adjacent-channel interference, are considered as pilot symbols. The generic symbol transmitted on the lth subcarrier of the kth OFDM block is denoted by $x[l,k]$. Defining $\mathbf{x}[k] \triangleq (x[0,k]\cdots x[L-1,k])^T$ as the vector that collects the data $\mathbf{a}[k]$ and
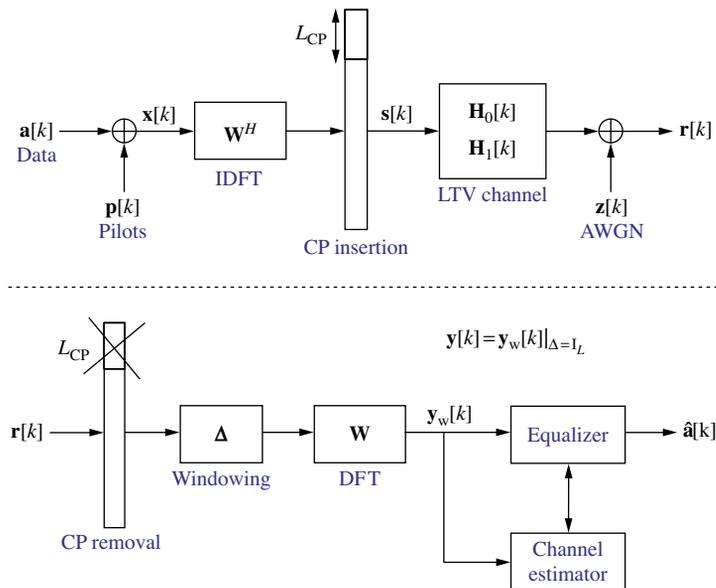
FIGURE 7.1

OFDM system model. Top: transmitter and channel. Bottom: receiver.

pilots $\mathbf{p}[k]$ of the kth block, i.e., $\mathbf{x}[k] = \mathbf{a}[k] + \mathbf{p}[k]$, the kth transmitted block $\mathbf{s}[k]$, of size $N = L + L_{CP}$, can be expressed as (Wang & Giannakis, 2000)

$$\mathbf{s}[k] = \mathbf{T}_{CP}\mathbf{W}^H\mathbf{x}[k]. \tag{7.1}$$

Here, $\mathbf{W}$ is the $L \times L$ unitary discrete Fourier transform (DFT) matrix, defined by $[\mathbf{W}]_{i,l} \triangleq \frac{1}{\sqrt{L}}e^{-j2\pi il/L}$, $0 \leq i, l \leq L - 1$, and $\mathbf{T}_{CP} \triangleq \left(\mathbf{I}_{CP}^T \ \mathbf{I}_L\right)^T$ is the $N \times L$ matrix that inserts the CP, where $\mathbf{I}_{CP}$ contains the last L_{CP} rows of the identity matrix $\mathbf{I}_L$. Thus, OFDM can be seen as a particular linearly precoded block transmission, with precoding matrix $\mathbf{T}_{CP}\mathbf{W}^H$.

After parallel-to-serial conversion, the signal stream $s[kN + n] \triangleq [\mathbf{s}[k]]_n$ is transmitted through a linear time-varying (LTV) multipath channel with discrete-time impulse response $h[n,m]$, where n is the time index and m is the time-delay (lag) index. We assume a finite impulse response LTV channel, i.e., $h[n,m]$ has zero entries outside $0 \leq m \leq M - 1$. Assuming time and frequency synchronization at the receiver side, the received samples can be expressed as

$$r[n] = \sum_{m=0}^{M-1} h[n,m]s[n-m] + w[n],$$

where $w[n]$ represents additive white Gaussian noise (AWGN). The N received samples relative to the kth OFDM block are grouped in the vector $\mathbf{r}[k]$, with $[\mathbf{r}[k]]_n = r[kN + n]$, thus obtaining

$$\mathbf{r}[k] = \mathbf{H}_0[k]\mathbf{s}[k] + \mathbf{H}_1[k]\mathbf{s}[k-1] + \mathbf{w}[k]. \tag{7.2}$$

Here, $\mathbf{H}_0[k]$ and $\mathbf{H}_1[k]$ are $N \times N$ matrices with elements $[\mathbf{H}_0[k]]_{n,m} = h[kN + n, n - m]$ and $[\mathbf{H}_1[k]]_{n,m} = h[kN + n, N + n - m]$:

$$\mathbf{H}_0[k] \triangleq \begin{pmatrix} h[kN,0] & 0 & \cdots & \cdots & 0 \\ \vdots & \ddots & \ddots & & \vdots \\ h[kN+M-1,M-1] & & \ddots & \ddots & \vdots \\ \vdots & \ddots & & \ddots & 0 \\ 0 & \cdots & h[kN+N-1,M-1] & \cdots & h[kN+N-1,0] \end{pmatrix},$$

$$\mathbf{H}_1[k] \triangleq \begin{pmatrix} 0 & \cdots & h[kN,M-1] & \cdots & h[kN,1] \\ \vdots & \ddots & & \ddots & \vdots \\ 0 & & \ddots & & h[kN+M-2,M-1] \\ \vdots & \ddots & & \ddots & \vdots \\ 0 & \cdots & 0 & \cdots & 0 \end{pmatrix}.$$

In obtaining (7.2), we have implicitly assumed that the block length N is greater than the channel order $M - 1$ so that ISI is possible only from the previous data block $\mathbf{s}[k-1]$. At the receiver, $\mathbf{r}[k]$ in (7.2) is left-multiplied by the matrix $\mathbf{R}_{CP} \triangleq \left(\mathbf{0}_{L \times L_{CP}} \ \mathbf{I}_L\right)$ that removes the CP. In what follows, we

assume $L_{CP} \geq M - 1$. Then, the ISI is completely eliminated, since $\mathbf{R}_{CP}\mathbf{H}_1[k]\mathbf{s}[k-1] = \mathbf{0}_{L \times 1}$ (Wang & Giannakis, 2000).

Next, the received signal is converted to the frequency domain by applying a DFT, as expressed by $\mathbf{y}[k] \triangleq \mathbf{W}\mathbf{R}_{CP}\mathbf{r}[k]$, which by (7.1) and (7.2) can be rewritten as

$$\mathbf{y}[k] = \mathbf{W}\mathbf{H}_T[k]\mathbf{W}^H\mathbf{x}[k] + \mathbf{W}\mathbf{R}_{CP}\mathbf{w}[k] = \mathbf{H}_F[k]\mathbf{x}[k] + \mathbf{z}[k]. \tag{7.3}$$

Here, $\mathbf{H}_T[k] \triangleq \mathbf{R}_{CP}\mathbf{H}_0[k]\mathbf{T}_{CP}$ is the $L \times L$ matrix that summarizes the LTV channel in the time domain, including CP insertion and removal, with elements expressed by

$$[\mathbf{H}_T[k]]_{n,m} = h[kN + L_{CP} + n, (n - m) \bmod L], \tag{7.4}$$

while $\mathbf{H}_F[k] \triangleq \mathbf{W}\mathbf{H}_T[k]\mathbf{W}^H$ is the $L \times L$ frequency-domain channel matrix, with elements expressed by

$$\begin{aligned}
[\mathbf{H}_F[k]]_{l+d,l} &= \frac{1}{L}\sum_{n=0}^{L-1}\sum_{m=0}^{L-1}[\mathbf{H}_T[k]]_{n,m}e^{-j2\pi(l(n-m)+dn)/L} \\
&= \frac{1}{L}\sum_{n=0}^{L-1}\sum_{m=0}^{M-1}h[kN + L_{CP} + n, m]e^{-j2\pi(lm+dn)/L},
\end{aligned} \tag{7.5}$$

where l represents the subcarrier index and d is the discrete Doppler index. Specifically, the off-diagonal elements of the lth column of $\mathbf{H}_F[k]$ represent the discrete Doppler spread associated with the lth subcarrier, which is responsible for the ICI induced by the lth symbol of the OFDM block on the other symbols.

Summarizing, clearly $\mathbf{H}_F[k]$ plays a crucial role, since it describes how the transmitted frequency-domain block $\mathbf{x}[k]$ is modified by the LTV channel. In addition, in (7.3), $\mathbf{z}[k] \triangleq \mathbf{W}\mathbf{R}_{CP}\mathbf{w}[k]$ is the frequency-domain noise, which is AWGN because $\mathbf{W}$ is unitary.

7.1.1.1 *LTI Channels and One-Tap Equalizers*

When either the channel time variation is absent, i.e., for LTI multipath channels, or it can be neglected, the channel impulse response (CIR) is constant over time. Hence, (7.4) becomes $[\mathbf{H}_T[k]]_{n,m} = h[0, (n - m) \bmod L]$, i.e., $\mathbf{H}_T[k] = \mathbf{H}_T$ is circulant and constant over the OFDM blocks. In this scenario, the CP not only eliminates the ISI, which could be removed by any kind of sufficiently long guard interval, e.g., by trailing zeros (Wang & Giannakis, 2000). In addition, the CP induces a time-domain circular convolution of the transmitted signal with the CIR, which corresponds to a scalar multiplication in the discrete frequency domain. Because the columns of the DFT matrix, which linearly precodes the OFDM data, are eigenvectors of circulant matrices, the eigenvalue decomposition of $\mathbf{H}_T$ is given by $\mathbf{H}_T = \mathbf{W}^H\mathbf{\Lambda}\mathbf{W}$. Consequently, $\mathbf{H}_F[k] = \mathbf{H}_F = \mathbf{\Lambda}$ is diagonal, which shows that in LTI channels there is no ICI. A continuous-time interpretation of OFDM systems is that, for every OFDM block, the lth symbol is transmitted in the frequency domain by a *sinc* function centered on the lth subcarrier. The zeros of this *sinc* function are located on the other equispaced subcarriers, which guarantees ICI-free

reception by DFT spectrum sampling. From (7.5), it is easy to derive

$$\lambda_{ll} \triangleq [\Lambda]_{l,l} = \sum_{m=0}^{M-1} h[0,m] e^{-j2\pi \, lm/L},$$

i.e., $\mathbf{H}_F$ contains on its diagonal the DFT of the CIR. Due to the diagonal frequency-domain channel matrix, the input–output relation can be expressed as

$$y[k,l] = \lambda_{ll} x[k,l] + z[k,l].$$

Hence, in OFDM systems, the equalization of LTI channels is rather simple and may be computed as $\hat{x}[k,l] = y[k,l]/\lambda_{ll}$ (Sari et al., 1995). This is usually referred to as *one-tap equalization*.

In general, the channel transfer function is estimated, for pilot locations, by $\hat{\lambda}_{ll} = y[k,l]/p[k,l]$ or by $\hat{\lambda}_{ll} = \frac{1}{K} \sum_{k=0}^{K-1} \frac{y[k,l]}{p[k,l]}$ when the pilot positions are constant for K OFDM blocks. Estimates of λ_{ll} for the data subcarriers are usually obtained by interpolating the channel values estimated for the pilot subcarriers (Ozdemir & Arslan, 2007).

7.1.1.2 **OFDM Standards**

In this section, we compare some popular wireless OFDM standards to appreciate their sensitivity to the Doppler spread induced by LTV channels. The OFDM standards under investigation are DVB-T/H (ETSI, 2004), DAB (ETSI, 2005), IEEE 802.11a (IEEE, 1999), and IEEE 802.16e (WiMAX) (IEEE, 2006). Clearly, the time variability of the channel, summarized by the channel coherence time T_c, should be compared with the duration of the OFDM block: standards with longer OFDM block duration are more sensitive to the Doppler effect; they feature bigger channel matrices $\mathbf{H}_T[k]$, whose diagonals display a larger time variability of the channel.

Dually, we can compare the maximum Doppler frequency ν_{max} with the subcarrier separation F: indeed, as it will be clarified in the next section, the ICI power is roughly a quadratic function of the normalized maximum Doppler shift $\vartheta_{max} \triangleq \nu_{max}/F$. As a consequence, robust standards have a small ϑ_{max}. This quantity can be calculated as

$$\vartheta_{max} = \frac{f_c}{F} \frac{\upsilon}{c_0},$$

where f_c is the carrier frequency, ν is the relative speed between transmitter and receiver, and c_0 is the speed of light.

For the IEEE 802.11a WLAN standard (IEEE, 1999), $F = 312.5$ kHz, while the frequency band is around 5 GHz. Specifically, for the maximum carrier frequency $f_c = 5.825$ GHz and speed $\upsilon = 100$ km/h, we obtain $\vartheta_{max} \approx 0.0017$.

For the IEEE 802.16e WiMAX standard (IEEE, 2006), the subcarrier separation depends on the ratio between the allocated bandwidth B and the number L of subcarriers as $F \approx \tilde{n}B/L$, where $\tilde{n}$ is a rational scaling factor between 1.12 and 1.152. Typical low values of B and L give $F \approx 9.77\tilde{n} \approx$ 10 kHz, which equals the value obtained for typical high values of B and L. Since the maximum carrier frequency is $f_c = 10.68$ GHz, for $\upsilon = 100$ km/h, we obtain $\vartheta_{max} \approx 0.089$. This value, which is roughly 50 times higher than for WLAN, explains why the channel time variation could be a problem for WiMAX, while it can be ignored in WLAN systems. Indeed, the emerging IEEE 802.11p standard

amendment for vehicular communications further increases the number of subcarriers with respect to IEEE 802.11a, without significantly degrading the Doppler resistance. The CP length is increased to guarantee ISI-free transmission in outdoor environments. The resulting loss in spectral efficiency is kept down by an increased duration of the IEEE 802.11p OFDM block.

For DVB-T/H (ETSI, 2004), the value of ϑ_{max} is highly dependent on the channel bandwidth B, which ranges from 5 to 8 MHz for different countries, on the carrier frequency f_c, and on the transmission mode, which determines the number of subcarriers L for a given bandwidth B. The available modes are Mode 2k ($L = 2048$), Mode 4k ($L = 4096$), and Mode 8k ($L = 8192$). In the following, we will focus on the 8k mode, which is the most sensitive to the Doppler spread. Assuming again $\upsilon = 100$ km/h, for $f_c = 230$ MHz, the normalized maximum Doppler shift is between $\vartheta_{max} \approx 0.019$ (for $B = 8$ MHz) and $\vartheta_{max} \approx 0.031$ (for $B = 5$ MHz). Hence, in this case, the Doppler effect for DVB-T/H 8k is less pronounced than for WiMAX. For $f_c = 862$ MHz, we have $\vartheta_{max} \approx 0.071$ for $B = 8$ MHz and $\vartheta_{max} \approx 0.11$ for $B = 5$ MHz. Therefore, in this second case, the sensitivity of DVB-T/H 8k to the channel time variation is similar to WiMAX. In addition, for $f_c = 1.492$ GHz, the performance degradation of DVB-T/H 8k is even higher than for WiMAX, since $\vartheta_{max} \approx 0.12$ for $B = 8$ MHz and $\vartheta_{max} \approx 0.20$ for $B = 5$ MHz. The results for $B = 6$ MHz and $B = 7$ MHz can be found in Table 7.1. With respect to Mode 8k, the subcarrier separation F of Modes 4k and 2k is the double and quadruple, respectively, and consequently, the values of ϑ_{max} are one-half and one-quarter of those for the 8k mode listed in Table 7.1.

Also for DAB (ETSI, 2005), and for its evolution known as T-DMB, we have to distinguish among different cases, depending on the carrier frequency f_c and the transmission mode. However, the transmission bandwidth is fixed to $B = 1.536$ MHz. The values of ϑ_{max}, listed in Table 7.2, show that the sensitivity of DAB Mode I to Doppler is similar to that of DVB-T/H Mode 8k with $B = 7$ MHz. The sensitivity of DAB Mode IV is similar to that of DVB-T/H Mode 4k, and the sensitivity of DAB Mode II is similar to that of DVB-T/H Mode 2k. Indeed, in all cases, the ratio of the number

Table 7.1 Normalized Maximum Doppler Shift ϑ_{max} for DVB-T/H (Mode 8k), Assuming $\upsilon = 100$ km/h.

	$B = 5$ MHz	$B = 6$ MHz	$B = 7$ MHz	$B = 8$ MHz
$f_c = 230$ MHz	$\vartheta_{max} \approx 0.031$	$\vartheta_{max} \approx 0.025$	$\vartheta_{max} \approx 0.022$	$\vartheta_{max} \approx 0.019$
$f_c = 862$ MHz	$\vartheta_{max} \approx 0.11$	$\vartheta_{max} \approx 0.095$	$\vartheta_{max} \approx 0.082$	$\vartheta_{max} \approx 0.071$
$f_c = 1492$ MHz	$\vartheta_{max} \approx 0.20$	$\vartheta_{max} \approx 0.16$	$\vartheta_{max} \approx 0.14$	$\vartheta_{max} \approx 0.12$

Table 7.2 Normalized Maximum Doppler Shift ϑ_{max} for DAB, Assuming $\upsilon = 100$ km/h

	Mode I, $L = 2048$	Mode IV, $L = 1024$	Mode II, $L = 512$	Mode III, $L = 256$
$f_c = 230$ MHz	$\vartheta_{max} \approx 0.021$	$\vartheta_{max} \approx 0.011$	$\vartheta_{max} \approx 0.0053$	$\vartheta_{max} \approx 0.0027$
$f_c = 862$ MHz	$\vartheta_{max} \approx 0.080$	$\vartheta_{max} \approx 0.040$	$\vartheta_{max} \approx 0.020$	$\vartheta_{max} \approx 0.010$
$f_c = 1492$ MHz	$\vartheta_{max} \approx 0.14$	$\vartheta_{max} \approx 0.069$	$\vartheta_{max} \approx 0.035$	$\vartheta_{max} \approx 0.017$

of subcarriers of DVB-T/H versus DAB is constant (equal to 4), and approximately equal to the bandwidth ratio.

7.1.2 Effects of Rapidly Time-Varying Channels

When the channel is LTV, the frequency-domain channel matrix $\mathbf{H}_F[k]$ in (7.5) is neither diagonal nor constant over successive OFDM blocks. Therefore, both the useful channel part and the ICI change from block to block. Let us split the frequency-domain channel matrix into two parts, as expressed by

$$\mathbf{H}_F[k] = \mathbf{Q}[k] + \boldsymbol{\Phi}[k],$$

where $\mathbf{Q}[k]$ is the diagonal part of $\mathbf{H}_F[k]$ and $\boldsymbol{\Phi}[k] \triangleq \mathbf{H}_F[k] - \mathbf{Q}[k]$ is the corresponding off-diagonal matrix. Then, (7.3) can be rewritten as

$$\mathbf{y}[k] = \mathbf{Q}[k]\mathbf{x}[k] + \boldsymbol{\Phi}[k]\mathbf{x}[k] + \mathbf{z}[k], \tag{7.6}$$

where the three terms on the right-hand side of (7.6) represent the useful signal, the ICI, and the AWGN, respectively. Since $q_{ll}[k] \triangleq [\mathbf{Q}[k]]_{l,l} = [\mathbf{H}_F[k]]_{l,l}$, from (7.5), the useful channel can be written as

$$q_{ll}[k] = \sum_{m=0}^{M-1} \left[\frac{1}{L} \sum_{n=0}^{L-1} h[kN + L_{CP} + n, m] \right] e^{-j2\pi lm/L}. \tag{7.7}$$

This is obtained as the DFT of the *time-averaged CIR*, which is the expression within the square brackets in (7.7). When the CIR varies rapidly with time, the time-averaged CIR in (7.7) decreases, because the elements $\{h[kN + L_{CP} + n, m]\}$ add incoherently. As a result, the average power of the frequency-domain useful channel (i.e., the power of the elements of $\mathbf{Q}[k]$) decreases. In addition, a rapid time variation of the CIR also leads to an increased ICI power in $\boldsymbol{\Phi}[k]$, as detailed in the next subsection.

7.1.2.1 ICI and SINR Analysis

Since conventional one-tap equalizers do not take the ICI into account, it is important to quantify the effect of the ICI on the decision variable. Herein, we present a statistical analysis of both the ICI and the SINR. For simplicity, in this subsection, we assume that only data symbols are transmitted, i.e., $x[k,l] = a[k,l]$, $\forall l, \forall k$. From (7.6), we obtain

$$y[k,l] = q_{ll}[k]a[k,l] + \sum_{d=0, d\neq l}^{L-1} \phi_{dl}[k]a[k,d] + z[k,l]. \tag{7.8}$$

Assuming that

1. data and noise terms have zero mean;
2. all data symbols on different subcarriers and in different OFDM blocks are uncorrelated and have equal mean power σ_a^2;
3. the LTV channel is wide-sense stationary with uncorrelated scattering (WSSUS) with normalized path loss, i.e., $\rho_{\mathbf{H}}^2$ defined in Chapter 1 is equal to one;
4. the noise is independent of the data and the channel;

then, the mean power received on the lth subcarrier of the kth OFDM block is expressed as

$$\sigma_y^2 \triangleq \mathsf{E}\{|y[k,l]|^2\} = \mathsf{E}\{|q_{ll}[k]|^2\}\sigma_a^2 + P_{\mathrm{ICI}}\sigma_a^2 + \sigma_z^2, \tag{7.9}$$

where $P_{\mathrm{ICI}} \triangleq \sum_{d=0,d\neq l}^{L-1}\mathsf{E}\{|\phi_{dl}[k]|^2\} = 1 - \mathsf{E}\{|q_{ll}[k]|^2\}$ is the ICI power normalized by the data power σ_a^2.

The value of P_{ICI} can be well approximated by assuming an infinite number of subcarriers. When the time-frequency correlation function $R_{\mathsf{H}}(\Delta t, \Delta f)$, defined in Chapter 1, is separable, i.e., $R_{\mathsf{H}}(\Delta t, \Delta f) = r_{\mathsf{H}}^{(2)}(\Delta t)r_{\mathsf{H}}^{(1)}(\Delta f)$, or equivalently when the scattering function $C_{\mathsf{H}}(\tau, \nu)$, defined in Chapter 1, is separable, i.e., $C_{\mathsf{H}}(\tau, \nu) = c_{\mathsf{H}}^{(1)}(\tau)c_{\mathsf{H}}^{(2)}(\nu)$, P_{ICI} can be expressed by (Li & Cimini Jr, 2001)

$$
\begin{aligned}
P_{\mathrm{ICI}} &= 1 - 2\int\limits_0^1 (1-x)\, r_{\mathsf{H}}^{(2)}\left(\frac{x}{F}\right)\mathrm{d}x \\
&= 1 - \int\limits_{-\nu_{\max}}^{\nu_{\max}} c_{\mathsf{H}}^{(2)}(\nu)\mathrm{sinc}^2\left(\frac{\pi\nu}{F}\right)\mathrm{d}\nu.
\end{aligned}
\tag{7.10}
$$

In this case, the ICI power does not depend on the delay power profile of the channel, whereas it depends on the Doppler power profile. For instance, in case of Jakes' Doppler power profile with $r_{\mathsf{H}}^{(2)}(\Delta t) = J_0(2\pi\vartheta_{\max}F\Delta t)$, where $\vartheta_{\max}$ is the normalized maximum Doppler shift, (7.10) becomes (Robertson & Kaiser, 1999)

$$
\begin{aligned}
P_{\mathrm{ICI}} &= 1 - {}_1F_2\left(\frac{1}{2}; \frac{3}{2}, 2; -(\pi\vartheta_{\max})^2\right) \\
&= 1 - 2\sum_{i=0}^{\infty}(-1)^i\frac{(\pi\vartheta_{\max})^{2i}}{(i!)^2\,(2i+1)\,(2i+2)} \\
&\approx \frac{\pi^2}{6}\vartheta_{\max}^2 - \frac{\pi^4}{60}\vartheta_{\max}^4 + \frac{\pi^6}{1008}\vartheta_{\max}^6,
\end{aligned}
\tag{7.11}
$$

where ${}_pF_q$ stands for the generalized hypergeometric function (Gradshteyn & Ryzhik, 1994). The ICI power can be calculated also for different Doppler power profiles, such as uniform, Gaussian, and the two-path model (Robertson & Kaiser, 1999). In particular, the two-path model characterizes the Doppler shift caused by a carrier frequency offset (CFO). In this case, we have

$$P_{\mathrm{ICI}} = 1 - \mathrm{sinc}^2(\pi\vartheta_{\max}) \approx \frac{\pi^2}{3}\vartheta_{\max}^2 - \frac{2\pi^4}{45}\vartheta_{\max}^4 + \frac{\pi^6}{315}\vartheta_{\max}^6. \tag{7.12}$$

It is noteworthy that the ICI power produced by a CFO is roughly twice the ICI power related to a classical Jakes' Doppler power profile and is quite close to the universal upper bound $P_{\mathrm{ICI}} \leq (\pi\vartheta_{\max})^2/3$ (Li & Cimini Jr, 2001).

When guard bands are present, the ICI power $\tilde{P}_{\mathrm{ICI}}[l] \triangleq \sum_{d\,\mathrm{active},d\neq l}\mathsf{E}\{|\phi_{dl}[k]|^2\}$ depends on the subcarrier index l. For subcarriers far away from the guard subcarriers, $\tilde{P}_{\mathrm{ICI}}[l] \approx P_{\mathrm{ICI}}$, expressed for instance by (7.11) or (7.12), while $\tilde{P}_{\mathrm{ICI}}[l] \approx P_{\mathrm{ICI}}/2$ for the edge subcarriers, since they receive

most interference from a single side only. The exact value of $\tilde{P}_{\text{ICI}}[l]$ can be determined by summing up the elements $\mathsf{E}\{|\phi_{dl}[k]|^2\}$ for all the indices $d \neq l$ corresponding to the active subcarriers, where (Schniter, 2004)

$$
\begin{aligned}
\mathsf{E}\{|\phi_{dl}[k]|^2\} &= \frac{1}{L^2} \sum_{m=-L+1}^{L-1} (L-|m|) r_{t,\mathbf{H}}[m] \mathrm{e}^{-j2\pi dm/L} \\
&= \left(\frac{\sin^2(\omega L/2)}{L^2 \sin^2(\omega/2)} * s_{\nu,\mathbf{H}}(\omega) \right) \Bigg|_{\omega=2\pi d/L}.
\end{aligned}
\tag{7.13}
$$

Observe that (7.13) is the DFT of the product of the triangular function $L - |m|$ and the discrete-time correlation $r_{t,\mathbf{H}}[m] \triangleq r_{\mathbf{H}}^{(2)}(m/(LF))$ of the channel, or, dually, the sampled version of the frequency-domain convolution of a squared digital-sinc function with the Doppler power profile of the discrete-time channel $s_{\nu,\mathbf{H}}(\omega) \triangleq \sum_{m=-\infty}^{\infty} r_{t,\mathbf{H}}[m] \mathrm{e}^{-j\omega m}$. This convolution destroys the zeros of the squared digital-sinc function and hence generates ICI. From (7.13), an important result is that $\mathsf{E}\{|\phi_{dl}[k]|^2\}$ rapidly decreases with increasing Doppler index d, because the squared-sinc function tends to zero quadratically. Hence, most of the ICI is due to only a few subcarriers, especially for small values of $\vartheta_{\max}$. Therefore, when the number L of subcarriers is large, $\tilde{P}_{\text{ICI}}[l] \approx P_{\text{ICI}}$ for almost all the subcarriers. It should be noted that (7.13) does not depend on the subcarrier index l, but only on the Doppler index d.

From (7.9), the SINR is expressed by

$$
\rho \triangleq \frac{\mathsf{E}\{|q_{ll}[k]|^2\}\sigma_a^2}{P_{\text{ICI}}\sigma_a^2 + \sigma_z^2} = \frac{1 - P_{\text{ICI}}}{P_{\text{ICI}} + \sigma_z^2/\sigma_a^2}.
$$

Hence, when the ICI is left uncompensated, the SINR cannot exceed the maximum value $\rho_{\max} = P_{\text{ICI}}^{-1} - 1$. When there are virtual subcarriers, the SINR on the lth subcarrier is expressed by $\rho_l = \frac{1-P_{\text{ICI}}}{\tilde{P}_{\text{ICI}}[l]+\sigma_z^2/\sigma_a^2}$, and the maximum SINR is $\rho_{\max} \approx 2(P_{\text{ICI}}^{-1} - 1)$ for the edge subcarriers.

7.1.2.2 BER Performance with One-Tap Equalizers

While the analysis of the ICI power is relatively straightforward, a theoretical BER analysis is quite difficult, apart from some specific cases. As a consequence, we assume that

1. a linear modulation scheme (e.g., PSK or QAM) is used;
2. the channel $h[n,m]$ is WSSUS with Rayleigh fading statistics;
3. a receiver with perfect time and frequency synchronization is used;
4. the one-tap equalizer for the lth subcarrier has perfect knowledge of the useful channel coefficient $q_{ll}[k]$.

First, we review some theoretical models for the uncoded BER, and then, we extend the discussion to the coded BER, which is usually investigated by simulations.

For theoretical purposes, the *power series model* of an LTV channel is often used (Bello, 1963). With this model, the time variation of the channel is represented by a Taylor series expansion, usually truncated to the first term, as expressed by

$$
h(t, \tau) \approx h(t_0, \tau) + h'(t_0, \tau)(t - t_0),
\tag{7.14}
$$

where t_0 is the time instant in the center of the OFDM block, and $h'(t_0, \tau) \triangleq \frac{\partial}{\partial t} h(t, \tau)\big|_{t=t_0}$. In the linear model (7.14), $h(t_0, \tau)$ stands for the useful component, and $h'(t_0, \tau)$ represents the slope of the channel time variability, assumed linear during the block interval. The approximation (7.14) is very accurate for relatively small time variability, e.g., when $\vartheta_{max} \leq 0.1$ (Chiavaccini & Vitetta, 2000), but can also be used when the Doppler spread is larger (Wang, Proakis, Masry, & Zeidler, 2006).

Since for Rayleigh fading $h(t_0, \tau)$ and $h'(t_0, \tau)$ are complex Gaussian and independent, the useful signal and the ICI will be independent, too. By dropping the block index k for simplicity, (7.8) becomes

$$y_l = q_{ll} a_l + i_l + z_l,$$

where the useful coefficient q_{ll} induced by $h(t_0, \tau)$ is Gaussian, and the ICI $i_l \triangleq \sum_{d=0, d \neq l}^{L-1} \phi_{dl} a_d$, related to $h'(t_0, \tau)$, is a Gaussian mixture.

When the number L of subcarriers is sufficiently high, due to the central limit theorem, the probability density function (pdf) of the ICI i_l can be well approximated as Gaussian, and hence, also $i_l + z_l$ is Gaussian. By means of this *Gaussian ICI approximation*, the BER can be obtained with standard approaches. For instance, for QPSK with Gray coding, the conditional bit error probability $\Pr\{\mathrm{Re}\{\hat{a}_l\} \neq \mathrm{Re}\{a_l\}|q_{ll}\}$ can be expressed as

$$\Pr\{\mathrm{Re}\{\hat{a}_l\} \neq \mathrm{Re}\{a_l\}|q_{ll}\} = Q\left(\sqrt{\frac{|q_{ll}|^2 \sigma_a^2}{\sigma_i^2[l] + \sigma_z^2}}\right), \tag{7.15}$$

where $Q(x) \triangleq \frac{1}{\sqrt{2\pi}} \int_x^\infty e^{-u^2/2} du$. The average of (7.15) over the Rayleigh pdf of $|q_{ll}|$ leads to

$$\Pr\{\mathrm{Re}\{\hat{a}_l\} \neq \mathrm{Re}\{a_l\}\} = \frac{1}{2}\left(1 - \sqrt{\frac{\rho_l}{\rho_l + 2}}\right), \tag{7.16}$$

where ρ_l is the SINR per symbol on the lth subcarrier. The same expression is also valid for the imaginary part. According to (7.16), the BER only depends on the SINR and does not depend on the delay power profile of the channel. Chiavaccini & Vitetta (2000) have shown that this approach is very accurate for QPSK when $L = 1024$. A similar approach has been used by Russell & Stüber (1995) to evaluate the symbol-error rate for 16-QAM. However, the numerical approximation of the symbol-error rate, expressed by $\Pr\{\hat{a}_l \neq a_l\} \approx 6.48/\rho_l$, is valid only for large SINR. Al-Gharabally & Das (2006) have used a Gaussian ICI approximation that also incorporates the effect of channel estimation errors.

An improved BER approximation can be obtained by avoiding the Gaussian ICI approximation. By denoting with $v_l \triangleq i_l/q_{ll}$ the ICI after equalization, the Gaussian mixture conditional pdf $f_{v_l|q_{ll}}(\mathrm{Re}\{v_l\}, \mathrm{Im}\{v_l\}|q_{ll})$ can be expressed as a two-dimensional Gram–Charlier series, whose coefficients depend on the joint moments of $\mathrm{Re}\{v_l\}$ and $\mathrm{Im}\{v_l\}$ (Wang, Proakis, Masry, & Zeidler, 2006); then, the conditional BER is obtained after series truncation, and the average over the statistics of q_{ll} can be done by means of semianalytical computation. Wang et al. (2006) have shown that a series truncation order equal to 4 produces a good accuracy for 16-QAM when $L = 128$. Interestingly, the Gram–Charlier series approach highlights that the uncoded BER is moderately dependent on the frequency selectivity of the channel. When truncated up to the second order, the Gram–Charlier series expansion reduces to the Gaussian ICI approximation.

For the coded BER, a theoretical characterization is rather difficult even for LTI channels, apart from some specific cases. Consequently, we only discuss some results obtained by simulations by Poggioni, Rugini, & Banelli (2008). We assume that the information bit sequence $b[i]$ is convolutionally encoded to obtain the coded bit sequence $c[j]$, whose length is $KA\log_2(N_a)$, where N_a is the constellation size, A is the number of data subcarriers, and K is the number of OFDM blocks within the interleaver time span. After interleaving and mapping, $P = L - A$ pilot symbols per block are added, and the KL resulting symbols are transmitted within K OFDM blocks. While for the uncoded BER the delay power profile of the channel has little importance, its effect on the coded BER is relevant, since channel coding is able to exploit the frequency selectivity of the channel. Moreover, when the interleaver time-span $T_{\text{int}} \triangleq K(1 + L_{\text{CP}}/L)/F$ is greater than the channel coherence time T_c, the OFDM system can benefit from the time selectivity of the channel.

While the coded BER performance highly depends on the specific channel encoder and interleaver, only a few channel parameters have a significant impact on the coded BER. To explain this point, we introduce the equivalent frequency-domain OFDM model (EFDOM) of Poggioni et al. (2008), which, combined with the specific channel encoder and interleaver, produces the same BER as the original OFDM model with LTV channels. Basically, the EFDOM is a simple approximate model obtained using only a reduced number of parameters, which are the most important for the coded BER. First, (7.8) is rewritten as

$$\underline{\mathbf{y}} = \underline{\mathbf{Q}}\underline{\mathbf{a}} + \underline{\mathbf{i}} + \underline{\mathbf{z}}, \tag{7.17}$$

where the underlined vectors, of size KL, are obtained by collecting the elements on the L subcarriers of the K OFDM blocks. In (7.17), the diagonal matrix $\underline{\mathbf{Q}}$ contains the useful part of the LTV channel, $\underline{\mathbf{a}}$ is the data vector, $\underline{\mathbf{i}}$ is the ICI vector, and $\underline{\mathbf{z}}$ stands for the AWGN vector. In order to speed up simulations for the coded BER, the EFDOM replaces (7.17) with

$$\underline{\mathbf{y}}^{(E)} = \underline{\mathbf{Q}}^{(E)}\underline{\mathbf{a}} + \sqrt{\varphi^{(E)}}\underline{\mathbf{i}}^{(E)} + \underline{\mathbf{z}}, \tag{7.18}$$

where $\underline{\mathbf{Q}}^{(E)}$ has the same statistical properties as $\underline{\mathbf{Q}}$, dictated by the delay power profile and by the Doppler power profile, $\underline{\mathbf{i}}^{(E)}$ is a Gaussian random vector with the same mean and the same covariance as $\underline{\mathbf{i}}$, and $\varphi^{(E)}$ is a real positive random variable that models the energy variability of the ICI with respect to its mean value. Specifically, $\varphi^{(E)}$ is a computer-generated random variable that has approximately the same pdf of the random variable

$$\varphi \triangleq \frac{\|\underline{\mathbf{i}}\|^2}{\mathsf{E}\{\|\underline{\mathbf{i}}\|^2\}} \approx \frac{\|\underline{\mathbf{i}}\|^2}{KLP_{\text{ICI}}\sigma_a^2},$$

whose pdf is well approximated by the pdf of the sum of exponential random variables (Poggioni et al., 2008). In the coded case, since K OFDM blocks are processed together, the time variability of the channel has a greater impact than in the uncoded case, where single blocks are separately considered. Therefore, in the coded case, the linear approximation (7.14) is not valid in general, and hence, the useful part of the channel $\underline{\mathbf{Q}}$ can be correlated with the ICI $\underline{\mathbf{i}}$. The EFDOM generates $\underline{\mathbf{Q}}^{(E)}$ and $\underline{\mathbf{i}}^{(E)}$ in (7.18) in such a way that $\rho_{\text{P}}^{(E)}$, defined as the correlation coefficient between $\|\underline{\mathbf{Q}}^{(E)}\underline{\mathbf{a}}\|^2$ and $\|\underline{\mathbf{i}}^{(E)}\|^2$, is equal to ρ_{P}, which is the correlation coefficient between $\|\underline{\mathbf{Q}}\underline{\mathbf{a}}\|^2$ and $\|\underline{\mathbf{i}}\|^2$. Indeed, simulation results
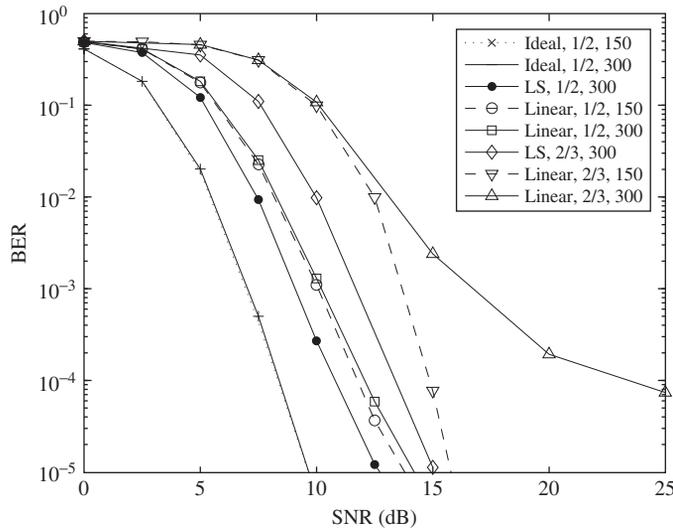
FIGURE 7.2

BER performance of DVB-H. In the legend, the first term indicates the type of channel estimation, the second term represents the code rate of the convolutional code, and the third term is the speed of the mobile receiver expressed in kilometer/hour.

have shown that the single coefficient ρ_P is able to summarize the whole correlation effect over the K blocks (Poggioni et al., 2008). For $K = 1$ (frequency-domain-only interleaver), ρ_P is practically zero for $\vartheta_{max} \leq 0.5$. Due to the EFDOM, fast simulation of coded OFDM standards is enabled.

Figure 7.2 shows the BER performance of DVB-H at the output of the Viterbi decoder. We consider Mode 2k ($L = 2048$) with carrier frequency $f_c = 800\,\text{MHz}$ and channel bandwidth $B = 8\,\text{MHz}$. For a mobile receiver with speed $\upsilon = 150\,\text{km/h}$, this corresponds to a normalized maximum Doppler shift $\vartheta_{max} \approx 0.025$. We assume QPSK modulation, a Rayleigh fading multipath channel with Jakes' Doppler power profile (Poggioni, Rugini, & Banelli, 2009), soft Viterbi decoding, and perfect time and frequency synchronization. The receiver assumes a time-invariant channel within the OFDM block. The CIR estimation is performed by interpolation or fitting of the frequency-domain channel estimates obtained on equispaced pilot subcarriers: in Fig. 7.2, *Linear* stands for linear interpolation, *LS* stands for least-squares fitting, and *Ideal* stands for perfect knowledge of the average CIR. Figure 7.2 shows that when the code rate of the convolutional encoder is 1/2, increasing the mobile speed from $\upsilon = 150\,\text{km/h}$ to $\upsilon = 300\,\text{km/h}$ produces a small performance degradation. On the contrary, when the code rate is 2/3, the performance degradation due to the increased mobile speed is significant, especially if the channel estimator employs linear interpolation. Using least-squares fitting instead of linear interpolation, a big performance improvement can be obtained, at the price of increased complexity.

Figure 7.3 illustrates the BER performance of DAB at the output of the Viterbi decoder. We consider Mode III ($L = 256$) with carrier frequency $f_c = 800\,\text{MHz}$ and channel bandwidth $B = 1.536\,\text{MHz}$. For a mobile receiver with speed $\upsilon = 150\,\text{km/h}$, this corresponds to a normalized maximum Doppler shift $\vartheta_{max} \approx 0.014$. We assume $\pi/4$-DQPSK modulation, a Rayleigh fading multipath channel with Jakes'
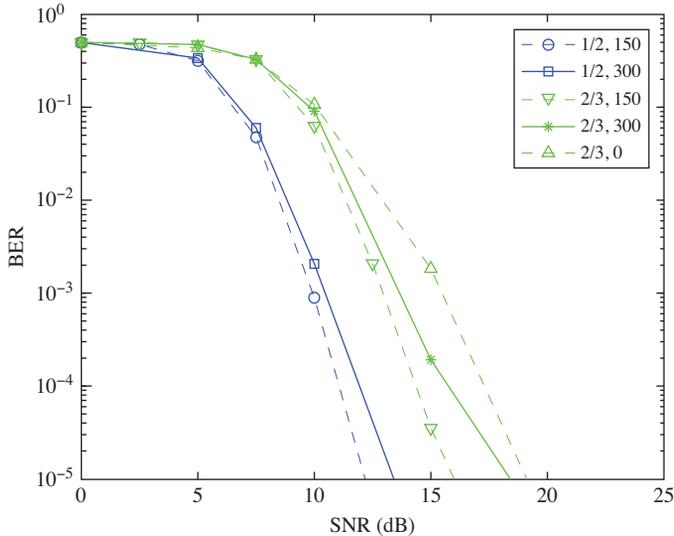
FIGURE 7.3

BER performance of DAB. In the legend, the first term represents the code rate of the convolutional code, and the second term is the speed of the mobile receiver expressed in kilometer/hour.

Doppler power profile, and soft Viterbi decoding (Poggioni et al., 2009). Differential demodulation is used. When increasing the mobile speed from $\upsilon = 0$ km/h to $\upsilon = 150$ km/h, the performance improves due to the time diversity gathered by the interleaver. However, when the mobile speed increases from $\upsilon = 150$ km/h to $\upsilon = 300$ km/h, the ICI causes a performance loss.

Additionally, Reed–Solomon encoding is incorporated in DVB-T/H and in T-DMB as outer code. A detailed performance comparison of DVB-T/H and T-DMB have been presented by Poggioni et al. (2009). For DVB-T/H, differently from the uncoded BER, the coded BER highly depends on the delay power profile of the channel (Poggioni et al., 2009). On the other hand, for T-DMB, the delay power profile of the channel has only a slight impact, because the effect of the time-domain interleaver is dominant (Poggioni et al., 2009).

7.1.3 MIMO-OFDM

We now extend the OFDM model with LTV channels to multiple-input multiple-output (MIMO) OFDM systems with M_T transmit antennas and M_R receive antennas. Denoting by $\mathbf{x}^{(j)}[k]$ the frequency-domain vector containing data and pilots of the jth transmit antenna, the vector transmitted from the jth antenna can be expressed as (see (7.1))

$$\mathbf{s}^{(j)}[k] \triangleq \mathbf{T}_{CP}\mathbf{W}^H\mathbf{x}^{(j)}[k].$$

The signal transmitted from the jth antenna arrives at the ith receive antenna after passing through an LTV channel with impulse response $h^{(i,j)}[n,m]$. We denote by M the maximum of the $M_T M_R$ maximum

discrete-time delay spreads. The vector received at the ith antenna can be expressed by (see (7.2))

$$\mathbf{r}^{(i)}[k] = \sum_{j=1}^{M_T} (\mathbf{H}_0^{(i,j)}[k]\mathbf{s}^{(j)}[k] + \mathbf{H}_1^{(i,j)}[k]\mathbf{s}^{(j)}[k-1]) + \mathbf{w}^{(i)}[k].$$

After CP removal and DFT, this becomes $\mathbf{y}^{(i)}[k] \triangleq \mathbf{WR}_{CP}\mathbf{r}^{(i)}[k]$, which is expressed by (see (7.3))

$$\mathbf{y}^{(i)}[k] = \sum_{j=1}^{M_T} \mathbf{H}_F^{(i,j)}[k]\mathbf{x}^{(j)}[k] + \mathbf{z}^{(i)}[k].$$

We now stack the vectors related to all the receive antennas in a single vector, denoted as $\underline{\mathbf{y}}[k] \triangleq \left(\mathbf{y}^{(1)T}[k]\cdots\mathbf{y}^{(M_R)T}[k]\right)^T$, and similarly for the transmit antennas, i.e., $\underline{\mathbf{x}}[k] \triangleq \left(\mathbf{x}^{(1)T}[k]\cdots\mathbf{x}^{(M_T)T}[k]\right)^T$, and we define the $LM_R \times LM_T$ matrix

$$\underline{\mathbf{H}}_F[k] \triangleq \begin{pmatrix} \mathbf{H}_F^{(1,1)}[k] & \cdots & \mathbf{H}_F^{(1,M_T)}[k] \\ \vdots & & \vdots \\ \mathbf{H}_F^{(M_R,1)}[k] & \cdots & \mathbf{H}_F^{(M_R,M_T)}[k] \end{pmatrix}.$$

The MIMO-OFDM system can then be described as

$$\underline{\mathbf{y}}[k] = \underline{\mathbf{H}}_F[k]\underline{\mathbf{x}}[k] + \underline{\mathbf{z}}[k]. \tag{7.19}$$

Expression (7.19) shows that in MIMO-OFDM systems, the ICI increases due to the presence of multiple transmit antennas. The ICI power, whose analysis has been presented by Stamoulis, Diggavi, & Al-Dhahir (2002), can be roughly estimated as M_T times the ICI for the single antenna case. In addition, as usual in MIMO schemes, there exists some inter-antenna interference (IAI). Despite the increased interference, multiple receive antennas provide additional degrees of freedom in order to mitigate both ICI and IAI.

In addition, we can stack the vectors related to K successive OFDM blocks, resulting in $\underline{\underline{\mathbf{y}}} \triangleq \left(\underline{\mathbf{y}}^T[0]\cdots\underline{\mathbf{y}}^T[K-1]\right)^T$ and $\underline{\underline{\mathbf{x}}} \triangleq \left(\underline{\mathbf{x}}^T[0]\cdots\underline{\mathbf{x}}^T[K-1]\right)^T$, and define the block diagonal matrix

$$\underline{\underline{\mathbf{H}}}_F \triangleq \begin{pmatrix} \underline{\mathbf{H}}_F[0] & & \mathbf{0} \\ & \ddots & \\ \mathbf{0} & & \underline{\mathbf{H}}_F[K-1] \end{pmatrix}.$$

We then obtain

$$\underline{\underline{\mathbf{y}}} = \underline{\underline{\mathbf{H}}}_F\underline{\underline{\mathbf{x}}} + \underline{\underline{\mathbf{z}}}. \tag{7.20}$$

In (7.20), the elements are ordered in such a way that first there is a change in the subcarrier index, then in the antenna index, and finally in the OFDM block index. However, this order can be changed by using suitable permutation matrices.

7.2 **ICI MITIGATION TECHNIQUES**

In this section, we present some common techniques for reducing the ICI produced by LTV channels. Some of these techniques have also been discussed in Chapter 6. Throughout this section, we assume that the LTV channel is unknown at the transmitter and perfectly known at the receiver. We first present techniques that make use of receiver processing only. These receiver-only techniques, which will be further divided into linear and nonlinear, are similar to those used for multiuser detection for code-division multiple-access (CDMA) systems. However, the specific structure of the ICI allows for some specific methods. Subsequently, we describe ICI mitigation techniques that employ transmitter preprocessing. These transmitter methods can be powerful, but in general are not compliant with the current OFDM standards. Finally, we extend the ICI mitigation techniques to MIMO-OFDM systems.

7.2.1 **Linear Equalization**

Among the receiver equalization methods, linear algorithms construct a soft data estimate by a linear combination of the received samples. For convenience, we rewrite (7.3) by dropping the OFDM block index as

$$\mathbf{y} = \mathbf{H}_F \mathbf{x} + \mathbf{z}, \tag{7.21}$$

where $\mathbf{y}$ represents the L-dimensional frequency-domain received vector, $\mathbf{H}_F$ is the $L \times L$ frequency-domain nondiagonal matrix that induces ICI, $\mathbf{x}$ is the frequency-domain transmitted vector, and $\mathbf{z}$ stands for the AWGN. Since the channel matrix $\mathbf{H}_F$ is assumed known at the receiver, to simplify the explanation, we assume that no pilot symbols are transmitted except for P guard subcarriers, which are consecutive and typically present in any OFDM standard. Here, P is assumed even. These guard bands correspond to the edge positions of the analog bandpass frequency-domain transmitted signal and hence to the central positions of the corresponding discrete-time baseband signal. For convenience, we reorder the subcarriers by a cyclic shift in such a way that the $A = L - P$ data positions are in the center. Denoting by $\mathbf{T}_{GB} \triangleq \left(\mathbf{0}_{A \times P/2} \ \mathbf{I}_A \ \mathbf{0}_{A \times P/2} \right)^T$ the $L \times A$ matrix that inserts the guard subcarriers, and by $\mathbf{a}$ the A-dimensional subvector of $\mathbf{x}$ containing the data symbols, we obtain $\mathbf{x} = \mathbf{T}_{GB}\mathbf{a}$. At the receiver, we can exclude the P virtual subcarriers by applying $\mathbf{R}_{GB} \triangleq \mathbf{T}_{GB}^T$, as expressed by $\mathbf{y}_A \triangleq \mathbf{R}_{GB}\mathbf{y}$. This becomes

$$\mathbf{y}_A = \mathbf{H}_A \mathbf{a} + \mathbf{z}_A, \tag{7.22}$$

where $\mathbf{H}_A \triangleq \mathbf{R}_{GB}\mathbf{H}_F\mathbf{T}_{GB}$ is the $A \times A$ ICI matrix relative to the data subcarriers and $\mathbf{y}_A$ ($\mathbf{z}_A$) is the A-dimensional received (AWGN) vector. Equalizers designed using the model (7.22) will be referred to as *block equalizers*, since the data subcarriers of the whole OFDM block are jointly equalized.

   As explained by (7.13), due to the structure of the Doppler spreading, the ICI on the lth subcarrier mainly comes from a few subcarriers. This means that the matrix $\mathbf{H}_A$ can be well approximated by a banded matrix $\mathbf{B}_A^{(D_b)}$, where D_b denotes the number of retained subdiagonals and, at the same time, superdiagonals of $\mathbf{H}_A$. An intuitive example of $\mathbf{B}_A^{(D_b)}$ is given in Fig. 7.4. Therefore, in the banded case, the block model (7.22) becomes

$$\mathbf{y}_A = \mathbf{B}_A^{(D_b)} \mathbf{a} + \mathbf{z}_A. \tag{7.23}$$
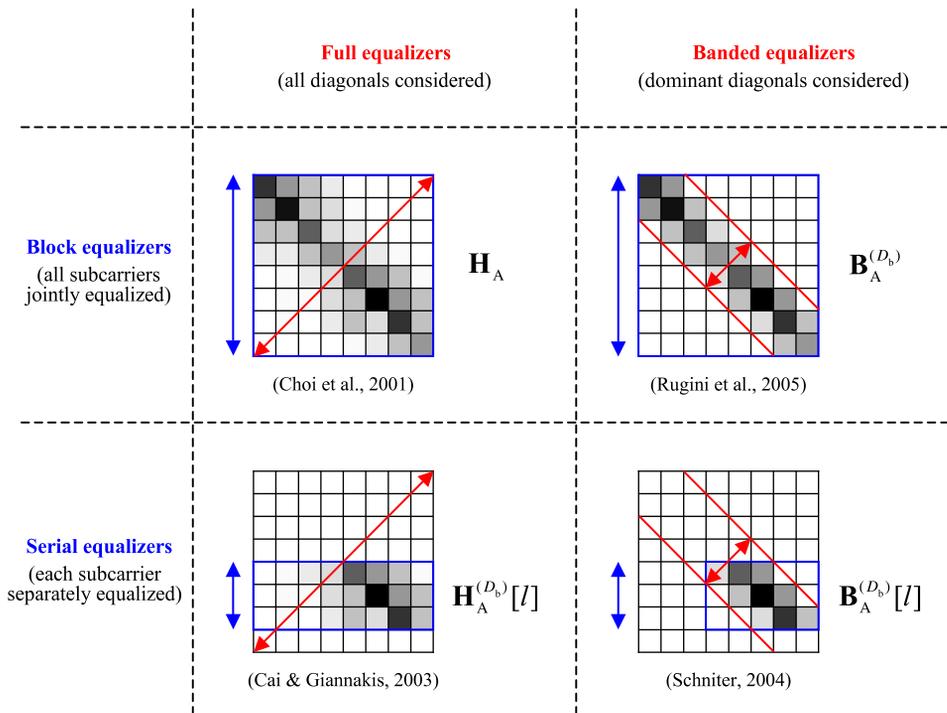
FIGURE 7.4

Possible approximations of the frequency-domain channel matrix. The gray intensity is proportional to the magnitude of the corresponding element.

The integer parameter D_b represents the (single-sided) discrete Doppler support that is used for equalization. Since the ICI coefficients $\mathsf{E}\{|\phi_{dl}[k]|^2\}$ in (7.13) have a rapid decay, the significant discrete Doppler support D is usually quite low. Anyway, we can select $D_b < D$ to reduce complexity. The value of D_b is usually chosen according to some empirical rules, such as proportionally to $\vartheta_{\max}$, or as the value that reduces the Frobenius norm $\|\mathbf{H}_A - \mathbf{B}_A^{(D_b)}\|_F^2$ below a given threshold. A common choice is $D_b = \lceil \vartheta_{\max} + D_0 \rceil$, where D_0 is a small nonnegative number (Schniter, 2004; Hwang & Schniter, 2006) (see also (6.6) in Chapter 6). This rule usually leads to $2D_b + 1 \ll L$, which allows for low-complexity equalization algorithms.[2]

It is noteworthy that the relations (7.22) and (7.23) only consider the A active subcarriers. When the equalizer considers all the L subcarriers, the frequency-domain channel matrix $\mathbf{H}_F$ can be approximated by a matrix with cyclically banded structure,[3] since the upper-right and the lower-left corners are significant (see Fig. 6.2(b) in Chapter 6). This effect, due to frequency-domain aliasing, disappears

---

[2]When the ICI mitigation support $2D_b + 1$ exceeds the channel length M, time-domain equalizers are less complex than frequency-domain equalizers (Hrycak & Matz, 2006).

[3]Cyclically banded matrices are also known as quasi-banded matrices.

in the presence of guard subcarriers, which cancel the first and the last columns of the channel matrix.

7.2.1.1 *Serial Equalizers*

Alternatively to the block models expressed by (7.22) and (7.23), a reduced model for the lth subcarrier can be exploited. Indeed, due to the banded structure of the channel matrix, the energy of the lth data symbol a_l mostly falls onto a subvector of $\mathbf{y}_A$ with size $2D_b + 1$, denoted by $\mathbf{y}_A^{(D_b)}[l] \triangleq \left(y_{l-D_b} \cdots y_l \cdots y_{l+D_b} \right)^T$, which can be expressed by

$$\mathbf{y}_A^{(D_b)}[l] = \mathbf{H}_A^{(D_b)}[l]\mathbf{a} + \mathbf{z}_A^{(D_b)}[l]. \tag{7.24}$$

Here, $\mathbf{H}_A^{(D_b)}[l]$ is the $(2D_b + 1) \times A$ submatrix of $\mathbf{H}_A$ that contains the rows with index from $l - D_b$ to $l + D_b$, as shown in Fig. 7.4, and $\mathbf{z}_A^{(D_b)}[l]$ is the AWGN subvector, defined similarly to $\mathbf{y}_A^{(D_b)}[l]$. The equalizers designed using (7.24) will be refered to as *serial equalizers*. Indeed, since (7.24) is valid for the lth subcarrier only, the data have to be equalized serially (sequentially). Including the band approximation, the serial model (7.24) becomes

$$\mathbf{y}_A^{(D_b)}[l] = \mathbf{B}_A^{(D_b)}[l]\mathbf{a}^{(D_b)}[l] + \mathbf{z}_A^{(D_b)}[l], \tag{7.25}$$

where $\mathbf{B}_A^{(D_b)}[l]$ is the $(2D_b + 1) \times (4D_b + 1)$ submatrix of $\mathbf{H}_A$ with row index from $l - D_b$ to $l + D_b$ and column index from $l - 2D_b$ to $l + 2D_b$ (see Fig. 7.4), and $\mathbf{a}^{(D_b)}[l] \triangleq \left(a_{l-2D_b} \cdots a_l \cdots a_{l+2D_b} \right)^T$.

In the context of LTV channel equalization for OFDM, different linear serial equalizers have been proposed so far. Indeed, although the reduced model (7.24) is suboptimal with respect to the full one (7.22), serial equalization deals with matrices and vectors with smaller dimension and hence reduces the memory requirements of the equalizer. One of the most popular serial equalizers is the zero-forcing (ZF) or least-squares (LS) banded approach of Jeon, Chang, & Cho (1999), which estimates the soft data as

$$\hat{a}_l = \mathbf{e}_{2D_b+1,D_b+1}^T \tilde{\mathbf{B}}_A^{(D_b)-1}[l]\mathbf{y}_A^{(D_b)}[l]. \tag{7.26}$$

Here, $\mathbf{e}_{m,n}$ is the nth column of $\mathbf{I}_m$, and $\tilde{\mathbf{B}}_A^{(D_b)}[l]$ is the $(2D_b + 1) \times (2D_b + 1)$ central block of $\mathbf{B}_A^{(D_b)}[l]$. Therefore, the ICI is completely eliminated, at the price of some noise enhancement, quantitatively summarized by the condition number of $\tilde{\mathbf{B}}_A^{(D_b)}[l]$. The computational complexity of banded linear serial equalizers can be reduced from $\mathcal{O}(D_b^3 A)$ to $\mathcal{O}(D_b^2 A)$ per block, using recursive inversion algorithms that compute $\tilde{\mathbf{B}}_A^{(D_b)-1}[l+1]$ by updating the already calculated $\tilde{\mathbf{B}}_A^{(D_b)-1}[l]$ (Cai & Giannakis, 2003).

To reduce the noise enhancement, serial equalizers based on the linear minimum mean-squared error (MMSE) criterion have been proposed. For instance, the nonbanded approach of Cai & Giannakis (2003) is expressed by

$$\hat{a}_l = \mathbf{e}_{A,l}^T \mathbf{H}_A^{(D_b)H}[l]\mathbf{R}_A^{(D_b)-1}[l]\mathbf{y}_A^{(D_b)}[l], \tag{7.27}$$

where $\mathbf{R}_A^{(D_b)}[l] = \mathbf{H}_A^{(D_b)}[l]\mathbf{H}_A^{(D_b)H}[l] + \gamma \mathbf{I}_{2D_b+1}$ and $\gamma = \sigma_z^2 / \sigma_a^2$ is the noise-to-signal ratio. With respect to (7.26), the approach in (7.27) produces an improved performance for two reasons: (1) differently from a ZF equalizer, an MMSE equalizer balances ICI reduction and noise enhancement; (2) there is no

band approximation error. Since nonbanded approaches model the out-of-band (OOB) elements of the ICI matrix, they have a larger computational complexity, which is $\mathcal{O}(D_b A^2)$ per block when recursive inversion is employed to obtain $\mathbf{R}_A^{(D_b)-1}[l+1]$ from $\mathbf{R}_A^{(D_b)-1}[l]$ (Cai & Giannakis, 2003).

A different linear serial equalizer has been proposed by Barhumi, Leus, & Moonen (2004) exploiting a basis expansion model (BEM) for both the LTV channel and the equalizer.[4] Using complex exponential basis functions, the linear equalizer of Barhumi et al. (2004) is modeled as banded with bandwidth parameter $\tilde{D}_b > D$, i.e., greater than the bandwidth of the channel matrix. The resulting complexity is $\mathcal{O}(\tilde{D}_b^2 A^2)$ per block.

7.2.1.2 *Block Equalizers*

In the literature, many linear block equalizers have been proposed, relying on either the LS or the MMSE criterion, sometimes exploiting the band approximation. LS and linear MMSE equalizers based on the full (nonbanded) model (7.22) have been proposed by Choi, Voltz, & Cassara (2001). However, due to the high complexity ($\mathcal{O}(A^3)$ per block), nonbanded block equalizers have limited applicability in OFDM systems with many subcarriers, such as DVB-T/H.

Indeed, in block equalization, a structured model of the frequency-domain channel matrix is essential to reduce the computational complexity of the equalizer and is instrumental for LTV channel estimation, too. For instance, by exploiting the band approximation, a linear block MMSE equalizer based on (7.23) can be expressed by (Rugini, Banelli, & Leus, 2005)

$$\hat{\mathbf{a}} = \mathbf{B}_A^{(D_b)H} \big(\mathbf{B}_A^{(D_b)}\mathbf{B}_A^{(D_b)H} + \gamma \mathbf{I}_A\big)^{-1}\mathbf{y}_A. \tag{7.28}$$

Since in (7.28) the matrix to be inverted is banded, the estimated data can be obtained by exploiting banded linear system solving techniques (such as band LDL^H factorization), whose complexity is $\mathcal{O}(D_b^2 A)$ like in the corresponding serial case. Figure 7.4 summarizes the four possible combinations that can be obtained by selecting a block or a serial equalizer and a banded or a full (nonbanded) equalizer. For each of the four models, different equalization criteria and structures are possible, including ZF, MMSE, and nonlinear equalizers.

Alternatively to direct equalization, block (and serial) equalization can be performed relying on *iterative linear equalization*. In contrast to iterative nonlinear equalization, which will be discussed in Section 7.2.2, iterative linear equalizers do not use hard decisions or nonlinearly modified (e.g., hyperbolic tangent) soft decisions of the data. Specifically, the matrix inversion in ZF or MMSE equalizers is avoided by performing an iterative procedure that produces an increasingly improved approximation of the exact result. For example, Li, Yang, Cai, & Gui (2003) have presented an iterative banded block ZF equalizer based on Jacobi iterations. Denoting by κ the iteration index, the received data vector is estimated as

$$\hat{\mathbf{a}}^{(\kappa)} = \mathbf{Q}_A^{-1}\big[\mathbf{y}_A - (\mathbf{B}_A^{(D_b)} - \mathbf{Q}_A)\hat{\mathbf{a}}^{(\kappa-1)}\big]$$
$$= \hat{\mathbf{a}}^{(\kappa-1)} + \mathbf{Q}_A^{-1}(\mathbf{y}_A - \mathbf{B}_A^{(D_b)}\hat{\mathbf{a}}^{(\kappa-1)}),$$

where $\mathbf{Q}_A$ is a diagonal matrix that contains the main diagonal of $\mathbf{B}_A^{(D_b)}$. The term $(\mathbf{B}_A^{(D_b)} - \mathbf{Q}_A)\hat{\mathbf{a}}^{(\kappa-1)}$ represents the soft ICI reconstructed from the previous iteration. Therefore, the ZF equalizer of

---

[4]We will discuss BEM techniques in the context of channel estimation in Section 7.3.1.

Li et al. (2003) implements a linear parallel ICI cancelation scheme. Since the matrix to be inverted is diagonal, each iteration requires very few computations. Moreover, the convergence of this algorithm to the exact solution $\hat{\mathbf{a}}^{(\infty)} = \mathbf{B}_A^{(D_b)-1}\mathbf{y}_A$ is always guaranteed. The speed of convergence can be slow, especially for some bad channel realizations. However, an acceleration of convergence can be achieved (Molisch, Toeltsch, & Vermani, 2007). The number of iterations and the choice of the initial estimate $\hat{\mathbf{a}}^{(0)}$ highly affect the approximation error of the final data estimate.

Undoubtedly, in block equalization, the system matrix is bigger than for serial approaches. As a consequence, a high condition number can be a significant issue. This problem can be reduced by using Tikhonov regularization, which adds a small term to γ in (7.28) to improve conditioning. Alternatively, γ can be replaced by the inverse modified SINR $\tilde{\rho}^{-1}$, where the modified SINR $\tilde{\rho} \triangleq \frac{1-P_{\mathrm{OOB}}^{(D_b)}}{P_{\mathrm{OOB}}^{(D_b)}+\gamma}$ is obtained by considering the elements of $\mathbf{H}_A$ within the main band as useful terms, and the OOB elements as effective ICI, as expressed by $P_{\mathrm{OOB}}^{(D_b)} \triangleq \|\mathbf{H}_A - \mathbf{B}_A^{(D_b)}\|_{\mathrm{F}}^2/A$. A third option is to employ an iterative equalization with implicit regularization: Taubӧck, Hampejs, Matz, Hlawatsch, & Grӧchenig (2007) have used an LSQR algorithm to perform iterative banded block ZF equalization constrained to the Krylov subspace generated by $\mathbf{B}_A^{(D_b)H}\mathbf{B}_A^{(D_b)}$ and $\mathbf{B}_A^{(D_b)H}\mathbf{y}_A$. In the LSQR algorithm, the conditioning improvement is obtained by early termination of the iterative algorithm, which also helps in saving complexity.

7.2.1.3 *Receiver Windowing*

Banded equalizers sometimes employ time-domain receiver windowing techniques to concentrate the ICI into the main band of $\mathbf{H}_A$ so that the band approximation is more accurate. This ICI shortening technique can be viewed as the dual of ISI channel shortening for single-carrier systems with LTI multipath channels. Receiver windowing is compatible with both serial (Schniter, 2004) and block (Rugini, Banelli, & Leus, 2006) approaches and can be used also in conjunction with nonlinear equalization. To examine receiver windowing, we define $\mathbf{y}_W \triangleq \mathbf{W}\boldsymbol{\Delta}\mathbf{R}_{\mathrm{CP}}\mathbf{r}$, where $\boldsymbol{\Delta}$ is the $L \times L$ diagonal matrix representing the time-domain windowing operation, performed before the DFT at the receiver. The OFDM signal model of (7.3) can then be replaced by

$$\mathbf{y}_W = \mathbf{W}\boldsymbol{\Delta}\mathbf{H}_T\mathbf{W}^H\mathbf{x} + \mathbf{W}\boldsymbol{\Delta}\mathbf{R}_{\mathrm{CP}}\mathbf{w} = \mathbf{H}_W\mathbf{x} + \mathbf{z}_W, \tag{7.29}$$

where $\mathbf{H}_W \triangleq \mathbf{W}\boldsymbol{\Delta}\mathbf{H}_T\mathbf{W}^H$ is the frequency-domain windowed channel matrix and $\mathbf{z}_W \triangleq \mathbf{W}\boldsymbol{\Delta}\mathbf{R}_{\mathrm{CP}}\mathbf{w}$ is the noise after windowing. It is interesting to note that $\mathbf{H}_W = \boldsymbol{\Gamma}\mathbf{H}_F$ and $\mathbf{z}_W = \boldsymbol{\Gamma}\mathbf{z}$, where $\boldsymbol{\Gamma} \triangleq \mathbf{W}\boldsymbol{\Delta}\mathbf{W}^H$ is a circulant filtering matrix that models receiver windowing (i.e., ICI shortening) in the frequency-Doppler domain. As a result of $\boldsymbol{\Gamma}$, the noise $\mathbf{z}_W$, though Gaussian, is no longer white. Obviously, by selecting $\boldsymbol{\Delta} = \mathbf{I}_L$, (7.29) reduces to classical OFDM and coincides with (7.3).

Receiver windowing does not affect the performance of nonbanded linear block equalizers, since it only performs a linear operation on the received signal. Nevertheless, when coupled with the band approximation, the OOB ICI energy, which is neglected by banded equalizers, can be greatly reduced, thereby improving performance considerably. From a performance viewpoint, a good window design criterion could be the minimization of the mean-squared error (MSE) on the decision variable. However, a closed-form solution to this minimization problem is hard to find. Therefore, common design criteria target the windowed matrix $\mathbf{H}_W$ rather than the MSE on the data. For instance, the *Max-Average*

SINR criterion of Schniter (2004) maximizes the average input SINR, expressed by

$$\rho_{\mathrm{IN}}^{(D_{\mathrm{b}})}(\boldsymbol{\Delta}) = \frac{\mathsf{E}\{\|\mathbf{B}_{\mathrm{W}}^{(D_{\mathrm{b}})}\|_{\mathrm{F}}^2\}}{\mathsf{E}\{\|\mathbf{H}_{\mathrm{W}} - \mathbf{B}_{\mathrm{W}}^{(D_{\mathrm{b}})}\|_{\mathrm{F}}^2\} + \sigma_z^2 \mathrm{tr}\{\boldsymbol{\Gamma}\boldsymbol{\Gamma}^H\}}, \tag{7.30}$$

where $\mathbf{B}_{\mathrm{W}}^{(D_{\mathrm{b}})}$ is the cyclically banded matrix that contains the $2D_{\mathrm{b}} + 1$ central diagonals of $\mathbf{H}_{\mathrm{W}}$. Of course, the maximization of (7.30) is subject to the window energy constraint $\mathrm{tr}\{\boldsymbol{\Delta}\boldsymbol{\Delta}^H\} = L$. Similarly, the *minimum band approximation error (MBAE)* criterion of Rugini et al. (2006) looks for the window that minimizes the OOB ICI energy $\mathsf{E}\{\|\mathbf{H}_{\mathrm{W}} - \mathbf{B}_{\mathrm{W}}^{(D_{\mathrm{b}})}\|_{\mathrm{F}}^2\}$, with the additional constraint that the window is the sum of $2D_{\mathrm{b}} + 1$ exponential (SOE) functions, as expressed by

$$\boldsymbol{\delta} \triangleq \mathrm{diag}\{\boldsymbol{\Delta}\} = \tilde{\mathbf{W}}^{(D_{\mathrm{b}})}\boldsymbol{\eta}^{(D_{\mathrm{b}})},$$

where $\tilde{\mathbf{W}}^{(D_{\mathrm{b}})}$ is an $L \times (2D_{\mathrm{b}} + 1)$ matrix that contains the first $D_{\mathrm{b}} + 1$ and the last D_{b} columns of $\mathbf{W}$, and $\boldsymbol{\eta}^{(D_{\mathrm{b}})}$ is a vector of size $2D_{\mathrm{b}} + 1$ containing the window coefficients. The MBAE solution $\boldsymbol{\eta}_{\mathrm{MBAE}}^{(D_{\mathrm{b}})}$ with the SOE constraint is the eigenvector that corresponds to the maximum eigenvalue of $\tilde{\mathbf{W}}^{(D_{\mathrm{b}})H}\mathbf{A}\tilde{\mathbf{W}}^{(D_{\mathrm{b}})}$, where $\mathbf{A}$ is an $L \times L$ Toeplitz matrix defined by

$$[\mathbf{A}]_{m,n} \triangleq r_{\mathrm{t},\mathsf{H}}[n - m]\frac{\sin\left(\pi\left(2D_{\mathrm{b}} + 1\right)(n - m)/L\right)}{L\sin\left(\pi\left(n - m\right)/L\right)}. \tag{7.31}$$

Hence, the window depends on the selected parameter D_{b}, and on the Doppler power profile (of the discrete-time channel) through the time-domain autocorrelation $r_{\mathrm{t},\mathsf{H}}[m]$ (see comments after (7.13)).

Other criteria than Max-Average SINR and MBAE-SOE are possible. For instance, different types of input SINR could be defined. The Max-SINR criterion of Schniter (2004) considers the instantaneous input SINR rather than the average input SINR. This translates into a window that depends on the LTV channel realization rather than on the LTV channel statistics. In this case, the window design must be repeated for each OFDM block. Das & Schniter (2007) have proposed a window design that considers: the elements on the main diagonal as useful signal; the other elements on the dominant diagonals as *don't-care* values; and the elements on the other diagonals as interference. The interference power also includes other disturbances, such as the ISI coming from the previous OFDM block when the CP is short or absent.

A nice feature of the window design with the SOE constraint is that the circulant matrix $\boldsymbol{\Gamma}$, which represents the frequency-domain noise after windowing, is cyclically banded (with bandwidth $2D_{\mathrm{b}} + 1$). This can be exploited for low-complexity equalization. The banded linear block MMSE equalizer (Rugini et al., 2006) can be expressed by (see (7.28))

$$\hat{\mathbf{a}} = \mathbf{B}_{\mathrm{WA}}^{(D_{\mathrm{b}})H}\left(\mathbf{B}_{\mathrm{WA}}^{(D_{\mathrm{b}})}\mathbf{B}_{\mathrm{WA}}^{(D_{\mathrm{b}})H} + \gamma\boldsymbol{\Gamma}_{\mathrm{A}}\boldsymbol{\Gamma}_{\mathrm{A}}^H\right)^{-1}\mathbf{y}_{\mathrm{WA}}, \tag{7.32}$$

where $\mathbf{B}_{\mathrm{WA}}^{(D_{\mathrm{b}})} \triangleq \mathbf{R}_{\mathrm{GB}}\mathbf{B}_{\mathrm{W}}^{(D_{\mathrm{b}})}\mathbf{T}_{\mathrm{GB}}$, $\boldsymbol{\Gamma}_{\mathrm{A}} \triangleq \mathbf{R}_{\mathrm{GB}}\boldsymbol{\Gamma}$, and $\mathbf{y}_{\mathrm{WA}} \triangleq \mathbf{R}_{\mathrm{GB}}\mathbf{y}_{\mathrm{W}}$ are obtained by excluding the guard bands. Since $\mathbf{B}_{\mathrm{W}}^{(D_{\mathrm{b}})}$ and $\boldsymbol{\Gamma}$ are cyclically banded, when the guard band on each side has size $P/2 \geq D_{\mathrm{b}}$, $\mathbf{B}_{\mathrm{WA}}^{(D_{\mathrm{b}})}$ is banded with bandwidth $2D_{\mathrm{b}} + 1$, and the matrix to be inverted in (7.32) is banded with bandwidth $4D_{\mathrm{b}} + 1$. Therefore, as in the absence of windowing, simple equalizers can be employed, with linear complexity in the number of subcarriers (Rugini et al., 2006).

The main advantage of receiver windowing lies in its extremely low additional complexity, despite the significant performance improvement. We note that good window designs require the knowledge of the channel statistics, such as the normalized maximum Doppler shift $\vartheta_{\max}$ and the shape of the Doppler power profile. In the absence of channel statistics, suboptimal windows can be employed, such as those used for spectral estimation (e.g., Hamming, Bartlett, Gaussian) (Harris, 1978), at the price of a reduced performance improvement. A performance comparison of different windows has been presented by Peiker, Dominicus, Teich, & Lindner (2008), assuming one-tap equalization and an additional cyclic extension (postfix).

7.2.1.4 *Performance-Complexity Trade-Off*

We now compare some representative linear equalizers in terms of simulated BER performance and computational complexity. We consider an OFDM system with $L = 128$ subcarriers, of which $A = 96$ are active, and QPSK modulated data. We assume a WSSUS Rayleigh fading channel with truncated exponential delay power profile $\mathsf{E}\{|h[n,m]|^2\} = \alpha e^{-0.6m}$, where α is a normalization constant. The channel length is chosen as $M = 9$, and consequently, the CP length is set to $L_{\mathrm{CP}} = 8$. Regarding the time variation of the channel, we assume a Jakes' Doppler power profile with $\vartheta_{\max} = 0.12$, i.e., the maximum Doppler frequency $\nu_{\max}$ is 12% of the subcarrier spacing F.

Figure 7.5 shows the BER performance of the following linear equalizers:

- Conventional one-tap equalizer;
- Full block ZF and MMSE equalizers (Choi et al., 2001);
- Banded serial ZF equalizer (Jeon et al., 1999);
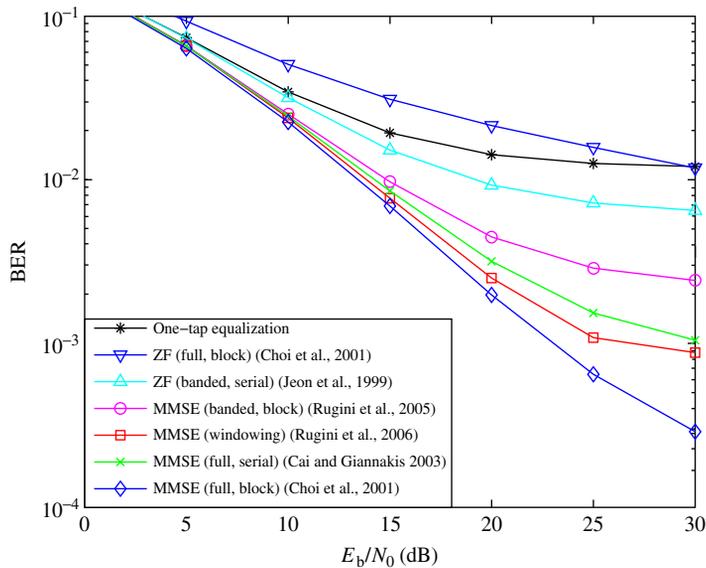
FIGURE 7.5

BER performance comparison of linear equalizers.

- Full serial MMSE equalizer (Cai & Giannakis, 2003);
- Banded block MMSE equalizer (Rugini et al., 2005) and its window-aided version (Rugini et al., 2006).

The matrix bandwidth parameter of banded equalizers is $D_b = 2$, i.e., only $2D_b + 1 = 5$ diagonals are considered. Similarly, serial equalizers only consider $D_b = 2$ subcarriers for each side, and hence, the observation vector length is $2D_b + 1 = 5$. The receiver window is designed using the MBAE-SOE criterion (Rugini et al., 2006), assuming perfect knowledge of the Doppler power profile. To avoid ill-conditioning problems at high SNR, in the absence of windowing, the banded block MMSE equalizer (Rugini et al., 2005) exploits a Tikhonov regularization, i.e., when the SNR $E_s/N_0 = \log_2(N_a)E_b/N_0$ exceeds 20 dB, the equalizer assumes a virtual SNR of 20 dB. All the equalizers exploit perfect channel-state information (CSI) at the receiver.

From the results of Fig. 7.5, it is clear that there exists a big performance gap between the ZF and MMSE equalizers. This confirms that doubly selective channels are ill conditioned, since an MMSE equalizer can be interpreted as a regularized ZF equalizer. Among the MMSE equalizers, the best performance is obtained by the full block approach of Choi et al. (2001), whose complexity per OFDM block is however cubic in the number of subcarriers. Therefore, the complexity for the full block MMSE equalizer of Choi et al. (2001) is $\mathcal{O}(A^2)$ per symbol, where $A^2 \approx 10^4$. The full serial MMSE equalizer of Cai & Giannakis (2003) is able to reduce the computational complexity to about $\mathcal{O}(D_b A)$ per symbol, with $(2D_b + 1)A \approx 500$, at a price of a modest performance loss. The banded block MMSE equalizer is able to significantly reduce complexity, since the number of complex operations per equalized symbol is $\mathcal{C} = 8D_b^2 + 22D_b + 4 = 80$ (Rugini et al., 2005), plus $2D_b + 1 = 5$ additional complex operations per symbol when windowing is included (Rugini et al., 2006).

Despite the lower complexity, the banded block MMSE equalizers maintain a good BER performance: specifically, due to the statistical CSI knowledge (summarized by the Doppler power profile), the window-aided banded block MMSE equalizer (Rugini et al., 2006) is able to outperform the full serial MMSE equalizer (Cai & Giannakis, 2003) with respect to both performance and complexity.

Figure 7.6 presents a BER performance comparison of banded block MMSE equalizers as a function of the normalized maximum Doppler shift $\vartheta_{\max}$, for the same scenario previously described, when $E_b/N_0 = 20$ dB. For comparison purposes, also the conventional one-tap equalizer and the full block MMSE equalizer (Choi et al., 2001) are considered. Clearly, to maintain a fixed performance, the matrix bandwidth size D_b should be increased as $\vartheta_{\max}$ grows, especially when receiver windowing is not used. However, the computational complexity increases quadratically with D_b, ranging from $\mathcal{C} = 8D_b^2 + 22D_b + 4 = 34$ complex operations per symbol when $D_b = 1$ to $\mathcal{C} = 220$ complex operations per symbol when $D_b = 4$. Moreover, when D_b increases, more matrix parameters have to be estimated, and hence, a more powerful channel estimator is required.

7.2.2 Nonlinear Equalization

A nonlinear equalizer estimates the data symbols by applying a nonlinear operation on the received vector. A typical configuration of a nonlinear equalizer consists of a first linear stage that produces some tentative data decisions and a second nonlinear stage that cancels the ICI using the tentative decisions. This configuration includes decision-feedback equalization, parallel ICI cancelation, successive ICI cancelation, and many other types of interference cancelation techniques. In addition, similarly to
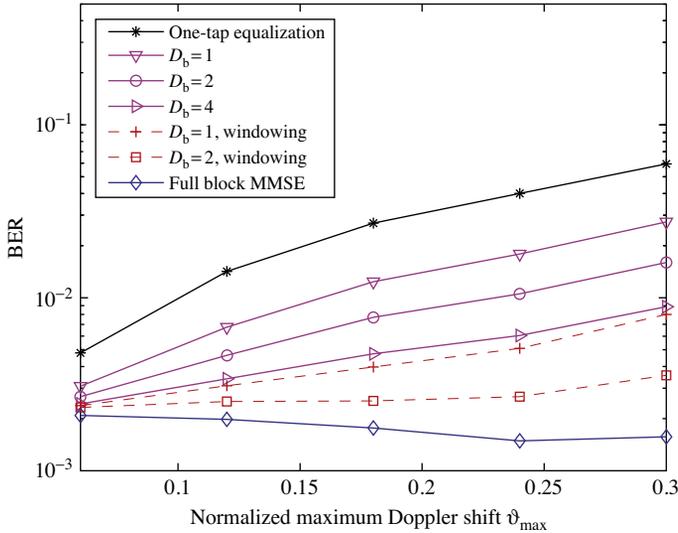
FIGURE 7.6

BER performance comparison of banded block MMSE equalizers.

multipath channel equalization for single-carrier systems, there exists a large variety of other nonlinear equalizer structures, including maximum-likelihood (ML) methods and turbo approaches. In all cases, as for linear equalizers, nonlinear equalizers can be classified as serial or block methods, banded or nonbanded approaches, window-aided or nonwindow-aided techniques.

Generally, a nonlinear equalizer performs better than a linear equalizer, although in many cases the computational complexity increases, especially for ML approaches. In the following, we review the most common techniques for OFDM systems with LTV channels.

7.2.2.1 *Decision-Feedback Equalizers*

Decision-feedback equalization (DFE) is characterized by a feedforward filter that reduces the ICI produced by the not-yet-detected symbols and a feedback filter that cancels the ICI produced by the already-detected symbols. For block equalizers, the soft-detected data can be expressed by

$$\hat{\mathbf{a}} = \mathbf{F}_F \mathbf{y}_A - \mathbf{F}_B \check{\mathbf{a}}, \tag{7.33}$$

where $\mathbf{F}_F$ is the $A \times A$ feedforward filter matrix, $\mathbf{F}_B$ is the $A \times A$ feedback filter matrix, and $\check{\mathbf{a}}$ contains the already-estimated hard-detected data symbols. Usually, the data symbols are detected sequentially, starting from the first (last) subcarrier; in this case, $\mathbf{F}_B$ should be strictly lower (upper) triangular, which guarantees that the not-yet-detected symbols are not fed back.

To design the DFE filters, the ZF or MMSE criterion can be used. Since a linear (ZF or MMSE) equalizer can be obtained as a degenerate case of DFE with $\mathbf{F}_B = \mathbf{0}_{A \times A}$, DFE approaches generally

outperform their corresponding linear counterparts. The main drawback of DFE is the error propagation due to the bad cancelation of an incorrectly detected symbol. Moreover, often the filter design optimistically assumes perfect (error-free) feedback, neglecting the error propagation.

For DFE, both serial and block approaches are possible. In block approaches, the two filters are jointly designed for all the subcarriers. Rugini et al. (2006) have presented some block MMSE DFE receivers that also incorporate a band approximation and receiver windowing. As in linear equalization, the band approximation is used to obtain $\mathbf{F}_F\mathbf{y}_A$ with reduced complexity. Moreover, $\mathbf{F}_B$ is also banded so that only $2D_b$ symbols are fed back, thereby reducing the error propagation. As a result, the computational complexity of the block DFE of Rugini et al. (2006) is $\mathcal{O}(D_b^2 A)$ per block. This complexity, which is lower compared to nonbanded approaches, is balanced by a performance loss that increases the error floor. However, also in the banded case, DFE outperforms linear equalization with basically the same complexity. The banded block DFE can also be coupled with receiver windowing, leading to a significant reduction of the error floor. However, the complexity is approximately doubled with respect to the nonwindowed DFE (Rugini et al., 2006).

In the serial case, the feedforward filter (different from subcarrier to subcarrier) acts on a few elements of the received vector, e.g., on $\mathbf{y}_A^{(D_b)}[l]$ in (7.25). One example is the serial MMSE DFE proposed by Cai & Giannakis (2003), where the filters are computed recursively from the filters used for the previously detected subcarrier. This recursive procedure reduces the complexity to $\mathcal{O}(D_b A^2)$ per block. A specific feature of the DFE of Cai & Giannakis (2003) relies on its cyclic ordering for successive cancellation. Consequently, the "best" subcarrier can be chosen as starting point instead of one of the edge subcarriers. This produces a clear connection with SIC equalizers, discussed in the following subsection.

7.2.2.2 *ICI Cancellers*

The concept of ICI cancelation, introduced for DFE above, is exploited also by other equalization structures, such as *successive interference cancellation (SIC)* equalizers. Also SIC equalizers have two stages, with the first producing tentative decisions and the second subtracting the regenerated ICI. However, differently from DFE, SIC equalizers perform an ordered ICI cancelation, in such a way that reliably detected subcarriers are detected first. Due to this subcarrier ordering, the probability of error propagation is reduced, especially for the first subtractions. However, a sorting procedure is necessary to establish the subcarrier ordering. This can be problematic for banded equalizers, since subcarrier sorting destroys the banded structure of the frequency-domain channel matrix.

In the technical literature, different options have been considered for the first tentative data detection: conventional one-tap equalization (Leung & Ho, 1998), nonbanded linear block MMSE equalization (Choi et al., 2001), and banded linear serial MMSE equalization (Kim & Park, 2006; Lu, Kalbasi, & Al-Dhahir, 2006). Also the detection order can be chosen using different criteria: postdetection SINR (Choi et al., 2001; Lu et al., 2006), magnitude of the diagonal elements of the channel matrix $\mathbf{H}_F$ (Kim & Park, 2006), and distance between soft and hard estimates produced by the first stage (Leung & Ho, 1998). The subcarrier order can be updated during the ICI subtraction, as in the nulling-canceling approach of Choi et al. (2001). This implies an increased complexity due to multiple sorting. In addition, many cancelation stages can be employed, as proposed by Leung & Ho (1998), who basically used an iterative nonlinear equalizer.

A closely related technique is *parallel interference cancelation (PIC)*, where the ICI of all the symbols is jointly canceled in a block fashion. The first estimate is typically obtained by one-tap MMSE equalization (Chen & Yao, 2004; Gorokhov & Linnartz, 2004) or by serial approaches (Chang, Han, Ha, & Kim, 2006; How & Chen, 2005). Banded cancelation is used to save complexity with small performance loss, since only the relevant ICI produced by a few subcarriers is subtracted. An improved PIC approach can be obtained by replacing the hard cancelation by reliability-based nonlinear soft cancelation (Molisch et al., 2007), where the hyperbolic tangent function is used to control the amount of ICI cancelation. Molisch et al. (2007) have also included a performance comparison with a SIC scheme.

Huang, Letaief & Lu (2005) have applied bit-interleaved coded modulation over multiple OFDM blocks. This scheme employs a reduced ML decoder obtained by approximating the LTV channel as constant over a single OFDM block. Since the reduced ML decoder neglects the ICI, its effectiveness is limited to low $\vartheta_{\max}$. For high Doppler spreads, the uncoded BER floor is too high, and the channel decoder even increases the BER. Therefore, Huang et al. (2005) have also included a PIC equalizer driven by a linear MMSE equalizer that works over multiple OFDM symbols.

Hybrid approaches that combine PIC with SIC are also possible, such as in *groupwise interference cancelation*. Basically, the set of subcarriers is split into a certain number of groups of subcarriers. Then, ICI cancelation within the group is performed in a parallel way, whereas the ICI among different groups is subtracted in a successive way. This reduces the ordering problem, because the number of groups is smaller than the number of subcarriers. Commonly, the groups contain consecutive subcarriers, but reliability-based subcarrier grouping criteria are sometimes used. Some examples of these techniques have been presented by Vogeler, Brötje, Klenner, Kühn, & Kammeyer (2004); Tran & Fujino (2005); Song, Kim, Nam, Yu, & Hong (2008); and Hampejs et al. (2009).

7.2.2.3 *Near-ML Equalizers*

Assuming the block model (7.22), the ML equalizer is expressed by

$$\hat{\mathbf{a}} = \arg\min_{\mathbf{s}} \|\mathbf{y}_A - \mathbf{H}_A \mathbf{s}\|, \tag{7.34}$$

where $\mathbf{s}$ is a generic possible data vector. Among the various approaches, the ML equalizer gives the best performance, since (7.34) minimizes the conditional probability of block error $\Pr\left\{\hat{\mathbf{a}} \neq \mathbf{a} | \mathbf{H}_A\right\}$. On the other hand, the ML approach is characterized by the worst complexity $\mathcal{O}(N_a^A)$, where N_a is the constellation size, i.e., the complexity is exponential in the number of active subcarriers A. Hence, a major goal is to find a low-complexity yet good approximation of the exact ML equalizer. In theory, most of the methods already developed for multiuser detection of CDMA signals could be employed, but the specific structure of the OFDM channel matrix and the potentially large number of subcarriers should be taken into account to avoid prohibitive complexity.

Using the band approximation $\mathbf{H}_A \approx \mathbf{B}_A^{(D_b)}$, Ohno (2005) proposed a banded block ML equalizer that reduces the equalization complexity up to $\mathcal{O}(D_b N_a^{2D_b+1} A)$. This is achieved by employing a Viterbi algorithm with a reduced number of surviving paths. However, in the case of a large constellation size N_a, complexity is still an issue. In addition, the Viterbi equalizer proposed by Ohno (2005) assumed white noise and therefore is not compatible with receiver windowing.

A second type of ML approximation consists in performing, for a specific subcarrier, a *local ML search* that only considers the neighboring subcarriers, with a philosophy that is similar to the blind

time-domain equalizer of Cui & Tellambura (2007). This approach can be regarded as the serial version of the banded ML equalizer.

Similarly, a third type of quasi-ML equalizers can be established by employing *sphere decoding* (see Section 3.8, Section 8.3.4 and references therein) or other *tree-search* techniques (see Section 6.3.2.4). For instance, Hwang & Schniter (2006) have applied a breadth-first search based on the T-algorithm, in a multicarrier system with transmitter and receiver windowing. This specific tree-search algorithm is coupled with a banded block MMSE DFE preprocessing with cyclic ordering, practically leading to ML performance with reduced complexity (below $\mathcal{O}(L^{2.4})$ per block) (Hwang & Schniter, 2006). Another tree-search algorithm has been investigated by Chow & Jeremic (2006).

As a fourth option, the optimization problem (7.34) can be relaxed to an equality-constrained *quadratic programming* problem, which is solved iteratively (Kou, Lu, & Antoniou, 2005). This approach can be extended to QAM as proposed by Zhang, Lu, & Gulliver (2007), which also reduces the equalization complexity by using a subspace constraint.

Mixed approaches are also possible. For instance, the groupwise approach of Feng, Minn, Yan, & Jinhui (2010) employs semidefinite relaxation to mitigate the ICI within a group of adjacent subcarriers and a PIC technique to reduce the ICI coming from the other groups of subcarriers.

7.2.2.4 *Iterative and Turbo Approaches*

Differently from the linear ones, iterative nonlinear equalizers perform nonlinear operations to iteratively update the data estimate. From this viewpoint, many ICI cancelation schemes that we described previously are also iterative. As a consequence, in this section, we describe those iterative nonlinear equalizers that have also other specific features.

As an example, equalization can be combined with channel estimation and with forward error correction decoding. Tomasin, Gorokhov, Yang, & Linnartz (2005) have presented an iterative channel estimator and a PIC equalizer that reuses the output of the convolutional decoder. The frequency-diversity gain provided by channel coding allows for a reliable ICI estimate, which produces improved performance (at least at medium-to-high SINR) but also increases the decoding delay. Joint equalization and channel estimation is also performed by Mostofi & Cox (2005).

A remarkable iterative structure is the turbo equalizer proposed by Schniter (2004), which is based on a window-assisted serial linear MMSE equalizer. In the equalizer of Schniter (2004), the symbol a_l is iteratively estimated using a linear MMSE (LMMSE) criterion, as expressed by

$$\hat{a}_l = \mu_l + \mathbf{e}_{4D_b+1,2D_b+1}^T \mathbf{B}_W^{(D_b)H}[l]\mathbf{R}_W^{(D_b)-1}[l]\big(\mathbf{y}_W^{(D_b)}[l] - \mathbf{B}_W^{(D_b)}[l]\boldsymbol{\mu}^{(D_b)}[l]\big). \tag{7.35}$$

Here, μ_l is the a priori mean of a_l, $\boldsymbol{\mu}^{(b)}[l] \triangleq \big(\mu_{l-2D_b} \cdots \mu_{l-1} \ 0 \ \mu_{l+1} \cdots \mu_{l+2D_b}\big)^T$ is the a priori mean of the data vector $\mathbf{a}^{(D_b)}[l]$ (except for the middle symbol, which is set to 0 instead of μ_l), $\mathbf{R}_W^{(D_b)}[l] \triangleq \mathbf{B}_W^{(D_b)}[l]\mathbf{V}^{(D_b)}[l]\mathbf{B}_W^{(D_b)H}[l] + \gamma\boldsymbol{\Gamma}^{(D_b)}[l]\boldsymbol{\Gamma}^{(D_b)H}[l]$ is the matrix to be inverted, with $\mathbf{V}^{(D_b)}[l] \triangleq$ diag$\big(v_{l-2D_b} \cdots v_{l-1} \ 1 \ v_{l+1} \cdots v_{l+2D_b}\big)$ the diagonal matrix that contains the a priori variances (except for a_l) and $\boldsymbol{\Gamma}^{(D_b)}[l]$ the $(2D_b + 1) \times L$ matrix obtained by selecting the rows of $\boldsymbol{\Gamma}$ from index $l - D_b$ to $l + D_b$. After LMMSE symbol estimation, the iterative procedure of Schniter (2004) updates the log-likelihood ratio (LLR) $L(a_l|\hat{a}_l)$, which is used to update the a priori means and variances (for QPSK, $\mu_l = \tanh(L(a_l|\hat{a}_l)/2)$ and $v_l = 1 - |\mu_l|^2$), to be used for symbol estimation in the next iteration. Different algorithms are possible depending on how the a priori quantities are updated: for

instance, in order to obtain $\hat{a}_l^{(\kappa)}$ in the κth iteration, (7.35) can use the a priori quantities calculated in the previous iteration $\left\{ \mu_{l-2D_b}^{(\kappa-1)}, v_{l-2D_b}^{(\kappa-1)}, ..., \mu_{l-1}^{(\kappa-1)}, v_{l-1}^{(\kappa-1)}, \mu_{l+1}^{(\kappa-1)}, v_{l+1}^{(\kappa-1)}, ..., \mu_{l+2D_b}^{(\kappa-1)}, v_{l+2D_b}^{(\kappa-1)} \right\}$, or it can employ also some a priori values already calculated in the current iteration $\left\{ \mu_{l-2D_b}^{(\kappa)}, v_{l-2D_b}^{(\kappa)}, ..., \mu_{l-1}^{(\kappa)}, v_{l-1}^{(\kappa)}, \mu_{l+1}^{(\kappa-1)}, v_{l+1}^{(\kappa-1)}, ..., \mu_{l+2D_b}^{(\kappa-1)}, v_{l+2D_b}^{(\kappa-1)} \right\}$. These two updating strategies correspond to a block-wise update and a serial-wise update, respectively. The simulation results of Schniter (2004) show that the serial-wise update produces a better performance, since the newly acquired a priori information is used as soon as it is available, thereby improving the convergence of the iterative algorithm. In both cases, the computational complexity is linear in the number of subcarriers and in the number of iterations.

Alternatively, the serial MMSE equalizer (7.35) can be replaced by a block MMSE equalizer that jointly calculates all the a priori values (Fang, Rugini, & Leus, 2008). In this case, only the block-wise a priori update is possible. Turbo block MMSE equalization can be related to probabilistic data association, which is commonly considered a quasi-ML technique. Indeed, in the presence of receiver windowing, the turbo block MMSE equalizer (Fang et al., 2008) outperforms the corresponding serial version, improving the BER performance at medium SNR. The computational complexity is similar to that of Schniter (2004).

Summarizing, many iterative ICI mitigation techniques have been presented in the literature, exploiting serial or block MMSE equalization, receiver windowing, and serial or block a priori LLR updating, sometimes incorporating channel estimation or channel decoding into the turbo loop. Obviously, performance and complexity highly depend on the type of iterative scheme and on the number of iterations. Therefore, a thorough comparison is difficult, except for some specific cases. A comparison between some selected schemes has been performed by Schniter (2004) and Fang et al. (2008). A general drawback of iterative nonlinear equalizers is the difficulty of a theoretical convergence analysis. Usually, the number of iterations is selected heuristically or by means of EXIT charts (ten Brink, 2001).

7.2.2.5 *Performance-Complexity Trade-Off*

First, we compare a linear block equalizer with a nonlinear block DFE approach. Both equalizers are designed using the MMSE criterion. The simulation scenario is that of Fig. 7.5, i.e., $L = 128$ subcarriers ($A = 96$ active), QPSK modulation, WSSUS Rayleigh channel with Jakes' Doppler power profile with $\vartheta_{\max} = 0.12$, and with truncated exponential delay power profile $\mathsf{E}\{|h[n,m]|^2\} = \alpha e^{-0.6m}$ of length $M = 9$. Banded equalizers use perfect CSI, $D_b = 2$, and Tikhonov regularization. MBAE-SOE windowing is employed.

Figure 7.7 shows the BER performance of three linear block MMSE equalizers (banded, window-aided, and full) and of three block MMSE DFE receivers (banded, window-aided, and full). The use of DFE produces a noticeable performance improvement. This improvement is more evident in the presence of windowing, e.g., when the computational complexity of DFE is roughly doubled with respect to linear approaches (Rugini et al., 2006).

We next compare two nonlinear approaches, focusing on iterative (turbo) MMSE equalizers. We again assume the simulation parameters of Fig. 7.7, except the channel length, which is $M = 17$ in this case, and the CP length $L_{CP} = 16$. Figure 7.8 displays the BER performance of two window-aided turbo banded MMSE equalizers using either a block approach (Fang et al., 2008) or a serial approach (Schniter, 2004). For both cases, $D_b = 2$ and MBAE-SOE windowing is adopted. The block equalizer employs Tikhonov regularization when the SNR E_s/N_0 exceeds 25 dB. For the serial equalizer, the
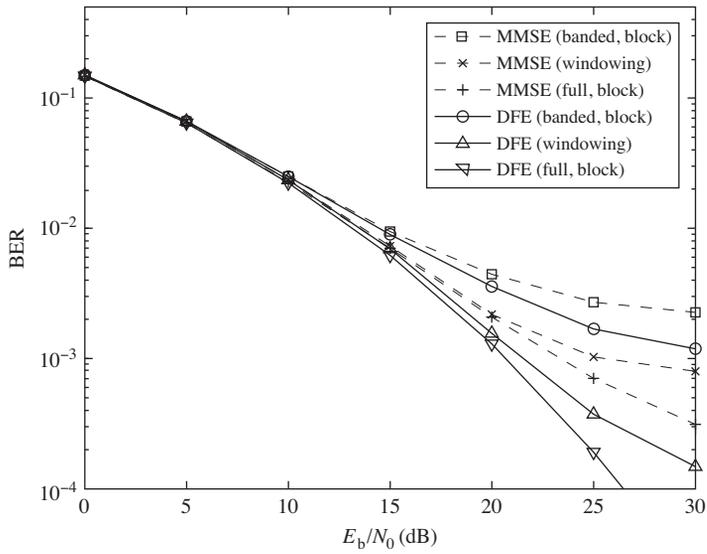
FIGURE 7.7

Block MMSE equalizers: BER performance comparison between linear and DFE versions.
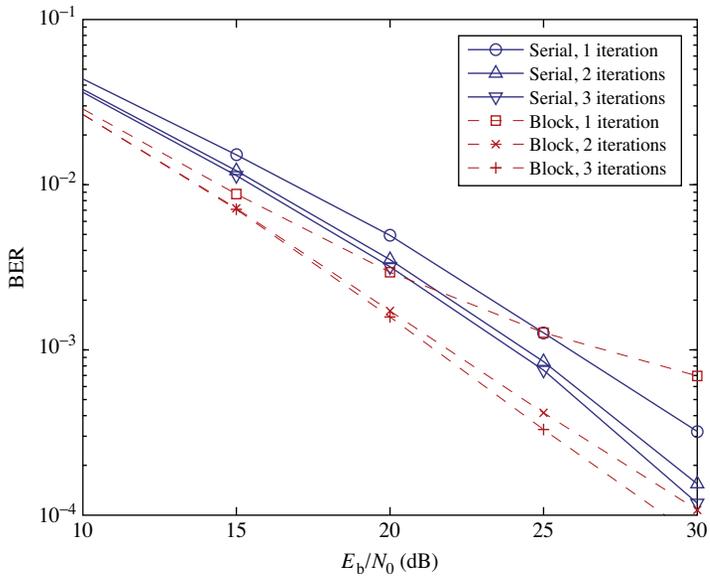
FIGURE 7.8

Iterative (turbo) banded MMSE equalizers: BER performance comparison between serial and block versions.

serial-wise LLR updating is considered, since it outperforms the block-wise LLR updating (Schniter, 2004). Figure 7.8 shows that the serial equalizer exhibits a slight performance loss at low SNR. This is mainly caused by the presence of windowing: since the window produces noise correlation across the subcarriers, considering only few subcarriers simultaneously is suboptimal. Block approaches jointly equalize all the subcarriers and therefore do not suffer from this loss. By focusing on the first iteration, obtained by linear equalization, it can be observed that the serial equalizer outperforms the block equalizer at very high SNR. This is mainly due to the ill-conditioning of the frequency-domain channel matrix, which is more problematic in the block case because of the larger size of the channel matrix. However, after the second iteration, the block equalizer is able to recover the gap and to outperform the corresponding serial version. More iterations improve the performance only slightly, in both cases. As far as complexity is concerned, both versions have linear complexity with respect to the number of subcarriers and the number of iterations. However, serial equalizers are more complex, with $\mathcal{C}_{\text{serial}} \approx 1.75\,\mathcal{C}_{\text{block}}$ when $D_{\text{b}} = 2$ and $\mathcal{C}_{\text{serial}} \approx 2.50\,\mathcal{C}_{\text{block}}$ when $D_{\text{b}} = 4$. On the other hand, serial equalizers deal with matrices of smaller size and hence in general are characterized by reduced memory requirements.

7.2.3 **Transmitter Preprocessing**

In Sections 7.2.1 and 7.2.2, we presented a broad overview of receiver processing techniques that are able to reduce the ICI power in CP-based OFDM systems with LTV channels. Current OFDM systems, which are designed for LTI channels, allow for the use of alternative receiver techniques when the channel is LTV. More refined approaches modify the OFDM transmission scheme in order to counteract the Doppler effect *before* the signal is received. As a result of transmitter processing, the need for equalization is highly reduced.

When the time variation of the channel is significant, it is not reasonable to assume full knowledge of the CSI at the transmitter. Therefore, CSI transmitter processing techniques used for LTI channels, such as ZF pre-equalization or Tomlinson–Harashima precoding, are not appropriate for LTV channels. However, statistical CSI knowledge of the WSSUS channel can be helpful.

In this section, we describe some common techniques to cope with the channel time variation at the transmitter. Some of these techniques have been originally proposed to counteract the ICI produced by a CFO, but have been successfully applied also to other types of Doppler distortions. We split these transmitter techniques into two categories: (1) data precoding, which only acts on the data to be transmitted, and (2) pulse shaping, which instead operates on the transmitted signal waveform. In general, data precoding requires a minor modification of current OFDM standards, since the precoded data can be transmitted by standard OFDM systems. On the other hand, pulse-shaping techniques require additional filtering at the transmitter and at the receiver.

7.2.3.1 *Data Precoding*

In OFDM, linear precoding of the frequency-domain data vector can result in a multipath diversity gain even in the absence of Galois-field channel coding (Wang & Giannakis, 2003). Similarly, data precoding across tones can be exploited aiming at ICI reduction (Zhang & Li, 2003; Zhao & Häggman, 2001). Two types of data precoding methods exist: redundant and nonredundant. Redundant linear precoding is performed by means of a tall $L \times A$ precoding matrix **P** applied to the data vector **a**.

By using (7.21), we can express the received data as

$$\mathbf{y} = \mathbf{H}_F \mathbf{P} \mathbf{a} + \mathbf{z}.$$

In other words, A data symbols share $L > A$ subcarriers. The most popular redundant precoding approach, known as *self-cancelation* or *polynomial cancelation coding* (Armstrong, 1999; Zhao & Häggman, 2001), exploits the ICI correlation of nearby subcarriers. For instance, the rate-1/2 scheme uses $\mathbf{P} = \mathbf{I}_{L/2} \otimes (1 \ {-}1)^T$, where $\otimes$ denotes the Kronecker product. Hence, the same symbol is transmitted on two consecutive subcarriers. At the receiver, the data symbols are estimated as

$$\hat{\mathbf{a}} = \mathbf{P}^H \mathbf{Q}^{-1} \mathbf{y} = \mathbf{P}^H \mathbf{Q}^{-1} \mathbf{H}_F \mathbf{P} \mathbf{a} + \mathbf{P}^H \mathbf{Q}^{-1} \mathbf{z},$$

where $\mathbf{Q} = \mathrm{diag}\{\mathbf{H}_F\}$, i.e., one-tap equalization is used. We note that the data received on two consecutive subcarriers are subtracted to recover the original data. Since there exists a strong correlation among nearby ICI elements of $\mathbf{H}_F$, significant ICI cancelation is achieved. In other words, the off-diagonal elements of the $L/2 \times L/2$ system matrix $\mathbf{P}^H \mathbf{Q}^{-1} \mathbf{H}_F \mathbf{P}$ are by far smaller than those of $\mathbf{Q}^{-1} \mathbf{H}_F$, which results in a reduced ICI. Consequently, significant performance gains are possible compared to convolutional coding (Zhao & Häggman, 2001), especially at high Doppler spread and at low SNR. As explained by Armstrong (1999) for CFO, this technique effectively eliminates the constant and linear components of the ICI variation over the rows of the frequency-domain channel matrix.

Even higher performance gains can be obtained by self-canceling more than two subcarriers. In general, $\mathbf{P} = \mathbf{I}_A \otimes \tilde{\mathbf{p}}$ is used, where $\tilde{\mathbf{p}}$ is a size-G vector obtained using the coefficients of the polynomial $p(x) = (1 - x)^{G-1}$ and $G \triangleq L/A$ (assumed integer) denotes the number of subcarriers per symbol (Zhao & Häggman, 2001). For instance, in the CFO case, $G = 3$ permits the elimination of the ICI up to the cubic component (Armstrong, 1999). The main drawback is the information rate reduction, which, however can be eliminated using higher-order constellations.

An extension of the self-cancelation method consists in precoding each data symbol over G consecutive carriers, which are used to transmit several frequency-shifted replicas of the same data symbol (Seyedi & Saulnier, 2005). The frequency-shift values can be integer (Zhao & Häggman, 2001) or noninteger numbers. Noninteger frequency-shifted data precoding can be implemented using frequency-domain upsampling and time-domain windowing, producing an additional computational complexity of only $\mathcal{O}(L)$ (Seyedi & Saulnier, 2005). The main drawback of this approach lies in the complexity of the window design, which requires a numerical maximization (Seyedi & Saulnier, 2005). Other ICI cancelation codes, based on capacity maximization, are investigated by Yun, Chung, & Lee (2007).

Nonredundant precoding techniques are commonly based on *correlative coding* (Zhao, Leclercq, & Häggman, 1998) and *partial response coding* (Zhang & Li, 2003), applied in the frequency domain. This corresponds to a square precoder $\mathbf{P}$ with triangular and banded structure applied to (modulo-precoded) data. Precoder designs that approximately minimize the ICI power have been presented by Zhang & Li (2003). Similarly to the time-domain case, the data detection can be performed using a per-subcarrier detector (Zhao et al., 1998) or a joint (ML-based) detector (Zhang & Li, 2003). This last case is more complex but provides significant ICI reduction (more than 4 dB).

7.2.3.2 *Pulse Shaping and Transmitter Windowing*

Pulse-shaping techniques use transmitter (and receiver) windows in order to reduce the sensitivity to ICI (Bölcskei, 2003; Haas & Belfiore, 1997; Hunziker & Dahlhaus, 2003; Kozek & Molisch, 1998; Matz, Schafhuber, Gröchenig, Hartmann, & Hlawatsch, 2007; Strohmer & Beaver, 2003). In this case, the signal waveform is modified without changing the transmitted data symbols. In addition to the reduced ICI, pulse-shaping techniques also provide additional robustness to frequency synchronization errors and reduce the spurious emissions into adjacent channels. To describe this set of techniques, it is useful to adopt a continuous-time model of the OFDM transmission. Similarly to (2.13) in Chapter 2, the transmitted signal can be expressed by

$$s(t) = \sum_{k=0}^{K-1}\sum_{l=0}^{L-1} a[k,l]g(t-kT)e^{j2\pi lFt},$$

where $a[k,l]$ is the data symbol transmitted on the lth subcarrier of the kth OFDM block, F is the subcarrier separation, T is the OFDM block duration, including a possible cyclic extension, and $g(t)$ is the transmitted pulse, which is rectangular in conventional OFDM systems. For simplicity, we assume that only data are transmitted. After passing through an LTV channel with continuous-time impulse response $h(t,\tau)$, the received signal is obtained as

$$r(t) = \int_{-\infty}^{\infty} h(t,\tau)s(t-\tau)d\tau + w(t),$$

which is demodulated by computing the inner products with the receiver pulse-shaped waveforms $\{\gamma(t-kT)e^{j2\pi lFt}\}$, as expressed by

$$y[k,l] = \int_{-\infty}^{\infty} r(t)\gamma^*(t-kT)e^{-j2\pi lFt}dt.$$

Conventional OFDM systems, which employ rectangular pulse shapes for both the transmitter pulse $g(t)$ and the receiver pulse $\gamma(t)$, are orthogonal for both ideal and LTI channels. Orthogonality means that in the absence of noise, $y[k,l]$ is a scaled version of $a[k,l]$ and hence does not contain any unwanted contribution from symbols $a[\tilde{k},\tilde{l}]$ with $(\tilde{k},\tilde{l}) \neq (k,l)$. In other words, ISI is absent, since $y[k,l]$ does not depend on $a[\tilde{k},\tilde{l}]$ with $\tilde{k} \neq k$, and also intra-block ICI is avoided,[5] because $y[k,l]$ does not depend on $a[k,\tilde{l}]$ with $\tilde{l} \neq l$. A necessary condition for orthogonality is $TF \geq 1$. For noiseless ideal channels, where the CP is not necessary, OFDM systems avoid the ISI by rectangular windowing, i.e., $g(t)$ is constant when $t \in [0,T]$ and $g(t) = 0$ elsewhere, and avoid the ICI by choosing $F = 1/T$. Indeed, the time-domain truncated complex exponentials $\{e^{j2\pi lFt}g(t), l = 0,...,L-1\}$ with $F = 1/T$ lead to a frequency-domain sinc-shaped waveform centered at $lF = l/T$ with zeros on a regular grid, at $l'F = l'/T$, $l' \neq l$, so that only a single *sinc* waveform contributes to the signal components at the frequency $lF = l/T$. In this case, $TF = 1$, i.e., the spectral efficiency is maximum. OFDM signals maintain their orthogonality even for LTI multipath channels, provided that a cyclic extension (or a guard interval) is inserted

---

[5]Note that we have included the inter-block ICI in the ISI component.

to guarantee ISI-free reception and $F = 1/T_U$, where T_U is the useful (CP-free) part of the signal. Note that in CP-based OFDM, orthogonality is maintained at the price of reduced spectral efficiency, due to the insertion of a guard period of duration $T_{CP} = T - T_U$, which makes $TF > 1$. However, the orthogonality of OFDM systems is lost in the case of LTV channels: the Doppler spread modifies the *sinc* waveforms by a frequency-domain convolution. Therefore, as explained after (7.13), the zeros of the resulting function do not fall on the regular frequency grid anymore, and consequently ICI arises. This ICI is significant for time-domain rectangular windowing in the case of LTV channels, since the *sinc* function decays only as $1/f$. On the contrary, using pulse-shaping (windowing) functions with better frequency-domain decay properties, less ICI would be introduced by Doppler spread, thereby decreasing the need for complex LTV equalization. Note that for LTV channels, OFDM systems with rectangular pulses avoid ISI, provided that a sufficiently long guard interval is inserted.

Let us first assume that the pulses $g(t)$ and $\gamma(t)$ have the same shape, as suggested by optimal (matched) filtering in AWGN. A first pulse-shaping approach to reduce the ICI for LTV channels, while maintaining orthogonality in the ideal case, is to use the Nyquist criterion (Muschallik, 1996) to design the pulses $g(t)$ and $\gamma(t)$. For instance, dually to the ISI mitigation principle for single-carrier transmissions, a time-domain raised cosine window, which decays as $1/f^3$, can be evenly split between transmitter and receiver. However, the decay rate is not the only factor that induces ICI mitigation (Tan & Beaulieu, 2004). Different kinds of orthogonal pulses have been proposed. The use of time-domain *sinc* pulse shapes makes the subcarrier spectrum rectangular and therefore is dual to conventional OFDM with rectangular pulses. This is the idealized version of the *filtered multitone* approach (Amini & Farhang-Boroujeny, 2009; Tonello & Pecile, 2008; Wang, Proakis, & Zeidler, 2007), which can use guard bands between subcarriers to completely eliminate the ICI in the case of LTV channels. Other designs adopt pulses that are well localized in both time and frequency. Some examples include the quasi-orthogonal pulses of Haas & Belfiore (1997), which are based on Hermite functions, and the scale-adapted pulses of Liu, Kadous, & Sayeed (2004), which are matched to the spread factor of the channel. Although the orthogonal approach is optimum for (nondispersive) AWGN channels, there is a price to be paid for the obtained ICI reduction. Indeed, any window with good spectral properties has a larger duration than the rectangular window, and consequently, an additional guard period is necessary to avoid ISI, thus reducing the spectral efficiency. Otherwise, inter-block orthogonality is lost, and ISI equalization is required even for nondispersive channels.

Another orthogonal scheme is the *lattice OFDM* approach of Strohmer & Beaver (2003), where the temporal locations of the OFDM blocks at a given subcarrier are staggered with respect to those at the two adjacent subcarriers. This gives rise to hexagonal lattices in the time-frequency plane, which is consistent with the sphere-packing principle. Well-localized pulses are designed by orthogonalization of Gaussian pulses, taking into account the shape of the channel scattering function $C_H(\tau, \nu)$. Since this scheme uses well-localized orthogonal pulses, $TF > 1$.

Let us now assume that the pulses $g(t)$ and $\gamma(t)$ have different shapes. *Biorthogonal* approaches rely on transmit and receive pulses $g(t)$ and $\gamma(t)$ that are characterized by the ambiguity function according to

$$A_{g\gamma}(kT, lF) \triangleq \int_{-\infty}^{\infty} g(t)\gamma^*(t - kT)e^{-j2\pi lFt}dt = \delta[k]\delta[l]. \qquad (7.36)$$

The key idea is that different transmit and receive pulses provide more degrees of freedom for ICI and ISI mitigation, at the price of a slightly reduced performance for idealized AWGN channels due to

mismatched receive filtering. Kozek & Molisch (1998) have proposed a transmit pulse design based on the maximization of the useful signal, leading to a large $|A_{g\gamma}(\tau,\nu)|^2$ wherever $C_\mathbf{H}(\tau,\nu)$ is large, while the receive pulse is chosen to fulfill the biorthogonality constraint. Matz et al. (2007) have proposed a receive pulse design that minimizes the ICI power (for a fixed transmit pulse).

Alternatively, *nonbiorthogonal* approaches are possible. In this case, different pulses $g(t)$ and $\gamma(t)$ that do not satisfy (7.36) are chosen. For instance, the joint transmit-receive pulse design of Matz et al. (2007) is obtained by disregarding the biorthogonality constraint. On the other hand, the pulse designs of Das & Schniter (2007) adopt an input SINR criterion that neglects the ICI due to nearby subcarriers, which is subsequently mitigated by an iterative banded nonlinear equalizer.

A different class of techniques is based on *offset QAM*, with real-valued pulses. The main advantage of pulse-shaped OFDM with offset QAM is the existence of well-localized functions even for $TF = 1$, which gives the maximum spectral efficiency. Some examples have been presented by Bölcskei (2003), Jung & Wunder (2007), Le Floch et al. (1995), and Vahlin & Holte (1995).

A totally different approach relies on using *chirp waveforms* for the "pulses" $g(t)$ and $\gamma(t)$. In this case, perfect ICI elimination is possible when the delay-Doppler spreading function of the channel is a straight line in the time-frequency plane (Barbarossa & Torti, 2001). Chirp approaches based on the fractional Fourier transform and on the affine Fourier transform have been presented by Martone (2001) and by Erseghe, Laurenti, & Cellini (2005), respectively.

7.2.4 **Extension to MIMO-OFDM**

The transmitter-based and receiver-based ICI mitigation methods discussed in the previous sections can be extended to MIMO-OFDM systems, using convenient methods to deal with the IAI arising from multiple receive antennas. The research on ICI mitigation in MIMO-OFDM systems is quite recent, and relatively few techniques have been proposed so far. Therefore, differently from the single-antenna case, a meticulous categorization of the proposed techniques is not opportune. In the following sections, we distinguish between ICI mitigation techniques proposed for spatial multiplexing systems, which aim at increasing the data rate, and techniques proposed for space-time-frequency coding systems, which seek to improve the performance.

7.2.4.1 *OFDM with Spatial Multiplexing*

In spatial multiplexing systems, different data symbols are transmitted from different antennas using shared frequency-time slots. Since (7.19) is formally similar to its single-antenna version (7.3), the equalization methods previously described can be used for MIMO-OFDM with minor modifications. For instance, a block linear MMSE equalizer has been investigated by Stamoulis et al. (2002), and a banded version that includes receiver windowing in the MBAE sense has been considered by Rugini & Banelli (2006). We note that linear equalization is appropriate only when $M_\mathrm{R} \geq M_\mathrm{T}$; otherwise there are not enough degrees of freedom for data recovery. Therefore, when $M_\mathrm{R} < M_\mathrm{T}$, nonlinear equalization or ICI cancelation is necessary.

Among the ICI cancelation techniques proposed in the literature, a simple approach consists in applying an iterative interference canceller with two stages: the first counteracts the ICI due to the Doppler spread, while the second reduces the IAI due to multiple transmit antennas. In the first stage, a banded PIC is usually adopted (Li, Li, & Vucetic, 2008; Song & Lim, 2006), while the second stage

could employ a VBLAST-like nulling-canceling method (Song & Lim, 2006) or a PIC with linear combining of the outputs of different iterations (Li et al., 2008). Alternatively, joint cancelation of both ICI and IAI can be performed by turbo banded approaches, as in the window-assisted equalizer of Rugini, Banelli, Fang, & Leus (2009) and in the turbo decoder of Liu & Fitz (2008).

Correlative coding has been extended to MIMO-OFDM by Zhang & Liu (2006). However, the data recovery by means of ML sequence estimation can be quite expensive when the number of subcarriers (and the number of transmit antennas) is large.

7.2.4.2 *OFDM with Space-Time-Frequency Coding*

It is well known that the BER performance for MIMO channels can be improved by space-time coding (STC). In MIMO-OFDM, there is an additional domain, and hence, space-frequency coding (SFC) or space-time-frequency coding (STFC) is also possible. The choice between STC and SFC depends on the channel selectivity: intuitively, STC is able to collect the time diversity, while SFC can gather the frequency diversity. STFC can collect both gains, but it requires additional processing.

OFDM is a type of block transmission, and consequently, most of the techniques proposed for MIMO-OFDM in LTV channels are based on block codes. Usually, the employed block codes are orthogonal, such as the well-known Alamouti code (Alamouti, 1998). However, the ICI induced by the channel Doppler spread destroys the code orthogonality, and consequently, Alamouti combining at the receiver is no longer equal to the ML detector. Lin, Chiang, & Li (2005) have compared different receiver combining methods (namely Alamouti, ZF, decision-feedback, and ML) for space-time block coding (STBC) and space-frequency block coding (SFBC).

Kim, Heath Jr, & Powers (2005) have proposed an STBC receiver that switches between decision-feedback and Alamouti combining. Fang, Leus, & Rugini (2006) have investigated a banded MMSE approach for STBC. For CFO distortions, a Tomlinson–Harashima precoder with partial CSI at the transmitter has been proposed by Fu, Tellambura, & Krzymien (2007). SFBC ICI self-cancelation codes are proposed in Dao & Tellambura (2005). The SFBC of Park & Cho (2005) is an Alamouti technique applied to a group of consecutive subcarriers, which contain redundant frequency-domain precoded data. Zhu, Wen, & Du (2008) have shown that space-time-frequency block coding (STFBC) outperforms STBC and SFBC, as expected by intuition.

7.3 TIME-VARYING CHANNEL ESTIMATION

Most of the described ICI mitigation techniques assume that the receiver knows the LTV channel. In rapidly time-varying scenarios, the channel estimation task is rather cumbersome because the CIR is not constant within the OFDM block. As a consequence, multiple parameter estimation is necessary for each channel path, and the estimation has to be repeated (or updated) for each OFDM block. Therefore, we include an overview of LTV channel estimation for OFDM (this issue is treated in more detail within Chapter 4). In this section, we first review the basis expansion model (BEM), which is one of the most popular channel models used for LTV channel estimation. Then, we describe some pilot-aided and data-aided channel estimation methods. An iterative channel estimation method based on turbo processing will also be considered.

7.3.1 **Basis Expansion Model of LTV Channels**

Since in the kth block the discrete-time LTV channel is expressed by $h[kN + L_{CP} + n, m]$, for $0 \leq n \leq L-1$ and $0 \leq m \leq M-1$, it is clear that ML parameters are required to represent the time-varying CIR, i.e., L values for each of the M channel paths. To reduce the number of parameters, each channel path can be modeled by a BEM in the kth OFDM block. With reference to the windowed channel, the BEM for the mth channel path is expressed by (Tsatsanis & Giannakis, 1996)

$$\Delta[n]h[kN + L_{CP} + n, m] = \sum_{i=0}^{I-1} c_{i,k}[m]u_i[n], \tag{7.37}$$

where $\Delta[n] \triangleq [\mathbf{\Delta}]_{n,n}$ is the nth window coefficient, I is the number of basis functions, $u_i[n]$ represents the ith basis function, which models the time variability, and $c_{i,k}[m]$ is the ith coefficient for the mth channel tap in the kth block. This approach reduces the number of channel parameters from ML to MI per block. By (7.37), the windowed time-domain channel matrix, which is obtained by multiplying the diagonal windowing matrix $\mathbf{\Delta}$ by $\mathbf{H}_T[k]$, can be expressed as

$$\mathbf{\Delta H}_T[k] = \sum_{m=0}^{M-1}\sum_{i=0}^{I-1} c_{i,k}[m]\mathbf{U}_{d,i}\mathbf{Z}_c[m] = \sum_{i=0}^{I-1}\mathbf{U}_{d,i}\mathbf{C}_{c,i}[k], \tag{7.38}$$

where $\mathbf{U}_{d,i}$ is a diagonal matrix defined by $\left[\mathbf{U}_{d,i}\right]_{n,n} \triangleq u_i[n]$, $\mathbf{Z}_c[m]$ is the $L \times L$ cyclic-shift matrix with ones in the mth lower diagonal and in the $(L-m)$th upper diagonal, and zeros elsewhere, and $\mathbf{C}_{c,i}[k] \triangleq \sum_{m=0}^{M-1} c_{i,k}[m]\mathbf{Z}_c[m]$. Consequently, the $L \times L$ windowed frequency-domain channel matrix $\mathbf{H}_W[k]$ in (7.29) can be expressed as

$$\mathbf{H}_W[k] = \sum_{m=0}^{M-1}\sum_{i=0}^{I-1} c_{i,k}[m]\mathbf{U}_{c,i}\mathbf{Z}_d[m] = \sum_{i=0}^{I-1}\mathbf{U}_{c,i}\mathbf{C}_{d,i}[k]. \tag{7.39}$$

In (7.39), $\mathbf{U}_{c,i} \triangleq \mathbf{W}\mathbf{U}_{d,i}\mathbf{W}^H$ is a circulant matrix that contains the (shifted version of the) discrete Doppler spectrum associated with the ith basis function, $\mathbf{Z}_d[m] \triangleq \mathbf{W}\mathbf{Z}_c[m]\mathbf{W}^H$ is diagonal with elements $[\mathbf{Z}_d[m]]_{n,n} = e^{j2\pi mn/L}$ that represent the frequency shift associated with the mth delay lag, and $\mathbf{C}_{d,i}[k] \triangleq \sum_{m=0}^{M-1} c_{i,k}[m]\mathbf{Z}_d[m] = \mathbf{W}\mathbf{C}_{c,i}[k]\mathbf{W}^H$ models the frequency selectivity associated with the projection of the multipath channel onto the ith basis function. Note that (7.38) and (7.39) are equivalent to (4.9) and (4.10), respectively, in Chapter 4. The specific structure of the channel matrix $\mathbf{H}_W[k]$ in (7.39) depends on the chosen basis. In any case, the structured model (7.39) opens the way to low-complexity algorithms for channel estimation and equalization.

Regarding the type of basis functions, a popular choice is to adopt $I = 2D + 1$ orthogonal critically sampled complex exponential (CCE) functions $u_i[n] = e^{j2\pi(i-D)n/L}$, $i = 0, \ldots, I-1$ (Tsatsanis & Giannakis, 1996) (see also (1.64) in Chapter 1), i.e., each function corresponds to a discrete Doppler frequency shift of i subcarriers. Thus, $\mathbf{U}_{c,i} = \mathbf{Z}_c[i - D]$, and hence, the basis functions produce a perfectly cyclically banded $\mathbf{H}_W[k]$ with $I = 2D + 1$ diagonals. In other words, the ICI support of CCE-BEM is finite (Tang, Cannizzaro, Leus, & Banelli, 2007). However, the CCE functions are periodic, with period equal to one OFDM block, while the time variability of the channel path is not periodic. As a consequence, the modeling error can be significant, especially at the edges of the block.

Alternatively, other types of basis functions can be employed. Another intuitive choice is to model the time variability by means of polynomials $u_i[n] = (n - \frac{L}{2})^i$ (Borah & Hart, 1999) (see also (1.66) in Chapter 1), which arise from the power series model of an LTV channel. In this case, the modeling error is negligible when the normalized maximum Doppler shift is low (Gorokhov & Linnartz, 2004; Tang et al., 2007). Other possible basis functions include oversampled complex exponential functions (Leus, 2004) (see also (1.65) in Chapter 1), discrete prolate spheroidal sequences (Zemen & Mecklenbräuker, 2005) (see also Section 1.6.1.3), and discrete Karhunen–Loève functions (Teo & Ohno, 2005, November/ December). The discrete Karhunen–Loève basis minimizes the MSE of the channel modeling, but it requires full statistical information about the Doppler power profile. On the other hand, the discrete prolate spheroidal basis assumes a flat Doppler power profile, and hence, it only requires knowledge of the maximum Doppler frequency. A comparison of the error produced by different basis functions has been performed by Zemen & Mecklenbräuker (2005) and Tang et al. (2007).

7.3.2 Training-Based Channel Estimation

When the LTV channel is represented by a BEM, the channel estimation problem reduces to the estimation of the BEM coefficients $c_i[m]$ from the received vector $\mathbf{y}_W[k]$ (and known pilots). With reference to the kth OFDM block, since $\mathbf{x}[k] = \mathbf{a}[k] + \mathbf{p}[k]$, (7.29) can be rewritten as

$$\mathbf{y}_W[k] = \mathbf{H}_W[k]\mathbf{x}[k] + \mathbf{z}_W[k] = \mathbf{H}_W[k]\mathbf{p}[k] + \mathbf{i}_W[k] + \mathbf{z}_W[k], \tag{7.40}$$

where $\mathbf{p}[k]$ is the known pilot or training vector, while $\mathbf{i}_W[k] \triangleq \mathbf{H}_W[k]\mathbf{a}[k]$ is the "interference" produced by the still unknown data vector $\mathbf{a}[k]$. From (7.39), the windowed channel matrix can be expressed by

$$\mathbf{H}_W[k] = \sum_{m=0}^{M-1}\sum_{i=0}^{I-1} c_{i,k}[m]\mathbf{U}_{c,i}\mathbf{Z}_d[m] = \mathbf{\Omega}(\mathbf{c}[k] \otimes \mathbf{I}_L), \tag{7.41}$$

where the BEM coefficients are collected in a single vector, as expressed by

$$\mathbf{c}[k] \triangleq (c_{0,k}[0] \cdots c_{I-1,k}[0] \cdots c_{0,k}[M-1] \cdots c_{I-1,k}[M-1])^T, \tag{7.42}$$

and $\mathbf{\Omega} \triangleq (\mathbf{\Omega}_{0,0} \cdots \mathbf{\Omega}_{I-1,0} \cdots \mathbf{\Omega}_{0,M-1} \cdots \mathbf{\Omega}_{I-1,M-1})$ with $\mathbf{\Omega}_{i,m} \triangleq \mathbf{U}_{c,i}\mathbf{Z}_d[m]$. Note that the vector $\mathbf{c}[k]$ defined in (7.42) is a permuted version of the vector defined in Chapter 4 after (4.8). From (7.40) and (7.41), using the identity $(\mathbf{c}[k] \otimes \mathbf{I}_L)\mathbf{p}[k] = (\mathbf{I}_{MI} \otimes \mathbf{p}[k])\mathbf{c}[k]$, we obtain

$$\mathbf{y}_W[k] = \mathbf{\Omega}(\mathbf{I}_{MI} \otimes \mathbf{p}[k])\mathbf{c}[k] + \mathbf{i}_W[k] + \mathbf{z}_W[k], \tag{7.43}$$

which clearly reveals the linear relationship between the received vector $\mathbf{y}_W[k]$ and the BEM coefficient vector $\mathbf{c}[k]$ to be estimated. Note that in general, the unknown vector $\mathbf{c}[k]$ also appears in the data-dependent term $\mathbf{i}_W[k]$, which can be rewritten as $\mathbf{i}_W[k] = \mathbf{\Omega}(\mathbf{c}[k] \otimes \mathbf{I}_L)\mathbf{a}[k] = \mathbf{\Omega}(\mathbf{I}_{MI} \otimes \mathbf{a}[k])\mathbf{c}[k]$.

In order to estimate the BEM coefficients, to reduce complexity, we can select only ω elements of $\mathbf{y}_W[k]$. Denoting by $\mathbf{S}[k]$ the $\omega \times L$ observation selection matrix constructed by selecting ω rows of $\mathbf{I}_L$, we obtain from (7.43)

$$\mathbf{y}_S[k] \triangleq \mathbf{S}[k]\mathbf{y}_W[k] = \mathbf{S}[k]\mathbf{\Omega}(\mathbf{I}_{MI} \otimes \mathbf{p}[k])\mathbf{c}[k] + \mathbf{i}_S[k] + \mathbf{z}_S[k], \tag{7.44}$$

where $\mathbf{i}_S[k] \triangleq \mathbf{S}[k]\mathbf{i}_W[k] = \mathbf{S}[k]\boldsymbol{\Omega}(\mathbf{c}[k] \otimes \mathbf{I}_L)\mathbf{a}[k]$ and $\mathbf{z}_S[k] \triangleq \mathbf{S}[k]\mathbf{z}_W[k]$. Obviously, the choice of the ω elements depends on the training pattern. Intuitively, we should select those elements of $\mathbf{y}_W[k]$ that mainly depend on the pilot vector $\mathbf{p}[k]$ and exclude those elements that mainly depend on the unknown data vector $\mathbf{a}[k]$.

In the following, we first review some LTV channel estimation techniques for OFDM when the MSE-optimal training for CCE-BEM channels is employed. Then, we describe some low-complexity channel estimation techniques for OFDM that use a suboptimal frequency-domain training without zero pilots, such as the DVB-T/H pilot pattern. Besides, we consider an adaptive frequency-domain approach based on both pilots and data.

7.3.2.1 *Estimation with Optimal Frequency-Domain Training*

Differently from LTI channels and from single-path LTV channels, where the MSE-optimal training is known (Tong, Sadler, & Dong, 2004) (see also Chapter 5), the MSE-optimal training for multipath LTV channels is known only for a specific channel model, i.e., CCE-BEM (Kannu & Schniter, 2008; Ma, Giannakis, & Ohno, 2003). For CCE-BEM LTV channels, the optimal training, known as frequency-domain Kronecker delta training, consists of M equispaced clusters placed in the frequency domain (Kannu & Schniter, 2008). Each cluster contains a single pilot subcarrier, surrounded by $2D$ zero subcarriers on each side (Kannu & Schniter, 2008). Therefore, the total number of training symbols in each OFDM block is $P = M(4D + 1) = M(2I - 1)$, while the other $A = L - P$ subcarriers can be used for the data symbols. Basically, the zero subcarriers should separate the data from the pilot clusters, in such a way that data and pilots remain orthogonal after the Doppler dispersion caused by the LTV channel. Indeed, a CCE-BEM channel of order $I = 2D + 1$ corresponds to a perfectly banded channel matrix that produces a maximum Doppler dispersion of $\pm D$ subcarriers. Therefore, a separation of $2D$ subcarriers between data and pilot clusters is the minimum amount that avoids pilot-data overlapping after the LTV channel. As a consequence, with this training pattern, a convenient choice is $\omega = MI$. This is obtained by selecting, for each of the M pilot clusters, only the $I = 2D + 1$ central elements. In this case, the interference $\mathbf{i}_S[k]$ is virtually absent, and (7.44) becomes

$$\mathbf{y}_S[k] \approx \mathbf{P}_S[k]\mathbf{c}[k] + \mathbf{z}_S[k], \tag{7.45}$$

where the system matrix $\mathbf{P}_S[k] = \mathbf{S}[k]\boldsymbol{\Omega}(\mathbf{I}_{MI} \otimes \mathbf{p}[k])$ is square. Hence, the BEM coefficients $\mathbf{c}[k]$ can be estimated by a deterministic approach, such as the LS estimator, expressed by (Kay, 1993)

$$\hat{\mathbf{c}}[k] = \mathbf{P}_S^{\#}[k]\mathbf{y}_S[k],$$

where $^{\#}$ denotes pseudoinverse. Alternatively, a stochastic approach can be used, such as the LMMSE estimator expressed by (Kay, 1993)

$$\hat{\mathbf{c}}[k] = \mathbf{C}_{\mathbf{cc}}\mathbf{P}_S^H[k](\mathbf{P}_S[k]\mathbf{C}_{\mathbf{cc}}\mathbf{P}_S^H[k] + \mathbf{C}_{\mathbf{z}_S\mathbf{z}_S}[k])^{-1}\mathbf{y}_S[k],$$

where $\mathbf{C}_{\mathbf{z}_S\mathbf{z}_S}[k] = \gamma\mathbf{S}[k]\boldsymbol{\Gamma}\boldsymbol{\Gamma}^H\mathbf{S}^T[k]$ is the noise covariance and $\mathbf{C}_{\mathbf{cc}}$ is the covariance matrix of the BEM coefficients, which is calculated as a function of the time correlation of the channel paths (Tang et al., 2007). In both the LS and LMMSE cases, the computational complexity of channel estimation is $\mathcal{O}(M^2I^2)$ per OFDM block.

To enhance the channel estimation performance, more observations $\omega > MI$ should be collected. In this case, differently from (7.45), the data-dependent interference cannot be neglected, and

$$\mathbf{y}_S[k] = \mathbf{P}_S[k]\mathbf{c}[k] + \mathbf{i}_S[k] + \mathbf{z}_S[k]. \tag{7.46}$$

Consequently, stochastic approaches should include the covariance $\mathbf{C}_{\mathbf{i}_S\mathbf{i}_S}[k]$ of the data-dependent interference $\mathbf{i}_S[k] = \mathbf{S}[k]\boldsymbol{\Omega}\,(\mathbf{c}[k] \otimes \mathbf{I}_L)\,\mathbf{a}[k]$, which however depends on the unknown $\mathbf{c}[k]$. Tang et al. (2007) have solved this problem by employing an iterative best linear unbiased estimator (BLUE), as expressed by

$$\hat{\mathbf{c}}^{(\kappa)}[k] = \big[\mathbf{P}_S^H[k]\big(\hat{\mathbf{C}}_{\mathbf{i}_S\mathbf{i}_S}^{(\kappa)}[k] + \mathbf{C}_{\mathbf{z}_S\mathbf{z}_S}[k]\big)^{-1}\mathbf{P}_S[k]\big]^{-1}\mathbf{P}_S^H[k]\big(\hat{\mathbf{C}}_{\mathbf{i}_S\mathbf{i}_S}^{(\kappa)}[k] + \mathbf{C}_{\mathbf{z}_S\mathbf{z}_S}[k]\big)^{-1}\mathbf{y}_S[k],$$

where κ is the iteration index, and

$$\hat{\mathbf{C}}_{\mathbf{i}_S\mathbf{i}_S}^{(\kappa)}[k] = \mathbf{S}[k]\boldsymbol{\Omega}\big(\hat{\mathbf{c}}^{(\kappa-1)}[k] \otimes \mathbf{I}_L\big)\mathbf{C}_{\mathbf{aa}}\big(\hat{\mathbf{c}}^{(\kappa-1)}[k] \otimes \mathbf{I}_L\big)^H\boldsymbol{\Omega}^H\mathbf{S}^T[k], \tag{7.47}$$

where $\hat{\mathbf{c}}^{(0)}[k] = \mathbf{0}_{MI\times 1}$ at the first iteration. As far as performance is concerned, the iterative BLUE produces a lower channel estimation MSE than an LMMSE estimator that neglects the covariance matrix of the interference (Tang et al., 2007). Iterative decision-feedback estimators are also possible: alternatively to (7.47), we can exploit a data-aided covariance estimate, as expressed by

$$\hat{\mathbf{C}}_{\mathbf{i}_S\mathbf{i}_S}^{(\kappa)}[k] = \mathbf{S}[k]\boldsymbol{\Omega}\big(\mathbf{I}_{MI} \otimes \hat{\mathbf{a}}^{(\kappa-1)}[k]\big)\mathbf{C}_{\mathbf{cc}}\big(\mathbf{I}_{MI} \otimes \hat{\mathbf{a}}^{(\kappa-1)}[k]\big)^H\boldsymbol{\Omega}^H\mathbf{S}^T[k],$$

which is based on the expression $\mathbf{i}_S[k] = \mathbf{S}[k]\boldsymbol{\Omega}(\mathbf{I}_{MI} \otimes \mathbf{a}[k])\mathbf{c}[k]$. Another option is to employ a data-dependent interference canceller that subtracts from (7.46) the term

$$\hat{\mathbf{i}}_S[k] = \mathbf{S}[k]\boldsymbol{\Omega}\big(\mathbf{I}_{MI} \otimes \hat{\mathbf{a}}^{(\kappa-1)}[k]\big)\hat{\mathbf{c}}^{(\kappa-1)}[k],$$

where $\hat{\mathbf{a}}^{(\kappa-1)}[k]$ is a (soft or hard) data estimate obtained by a channel equalizer at the previous iteration.

A different approach relies on adaptive channel estimation. As an example, Kalman filtering and recursive least-squares methods, discussed by Cannizzaro, Banelli, & Leus (2006), exploit the time correlation of the channel over successive OFDM blocks. In addition, adaptive techniques are able to track the variability of the channel statistics and are therefore suitable for nonstationary environments. In case of frequent changes of the channel statistics, a robust approach based on H_∞ filtering may be appropriate (Banelli & Rugini, 2010).

7.3.2.2 *Estimation with Suboptimal Training*
Current OFDM-based systems, such as DVB-T/H, IEEE 802.11a, and IEEE 802.16e (WiMAX) (ETSI, 2004, 2005; IEEE, 1999, 2006), are designed for LTI or slowly time-varying channels, and therefore, their training patterns are different from the frequency-domain Kronecker delta pattern discussed so far. Usually, packet-based systems such as IEEE 802.11a employ a time-domain preamble, mainly used for time synchronization and channel estimation, and few frequency-domain pilots, mainly used for CFO compensation and tracking. On the other hand, continuous systems such as DVB-T/H usually

employ only frequency-domain pilots, whose locations change with the OFDM block index. In these cases, the frequency-domain pilots are adjacent to the data symbols, and therefore, significant ICI is present when the channel is rapidly time varying.

In order to estimate LTV channels by means of (nonzero-guarded) frequency-domain pilots, such as in DVB-T/H, many techniques have been proposed. Usually, these techniques first collect information from consecutive OFDM blocks; then, for the pilot positions, they estimate a sampled version of the LTV channel in the joint time-frequency domain; and finally, for the data positions, they use interpolation techniques to recover the whole LTV channel. To keep the complexity low, the channel is sometimes modeled as constant within a single OFDM block. This assumption actually leads to the estimation of the *time-averaged CIR* (expressed inside the square brackets in (7.7)). Since the ICI is neglected, the time variation of the channel within the OFDM block is ignored. However, the time variation can subsequently be reconstructed by interpolating the estimated channel values corresponding to consecutive OFDM blocks.

Among the proposed techniques, we can distinguish between batch algorithms (Hoeher, Kaiser, & Robertson, 1997; Hutter, Hasholzner, & Hammerschmidt, 1999; Lai & Chiueh, 2006) and adaptive algorithms (Sanzi & Speidel, 2000; Schafhuber & Matz, 2005; Schafhuber, Matz, & Hlawatsch, 2003, April). In addition, the two-dimensional interpolation can be performed either jointly in the time-frequency domain (Hoeher et al., 1997; Schafhuber & Matz, 2005; Schafhuber et al., 2003, April) or separately, as a cascade of two one-dimensional interpolators (Hutter et al., 1999; Lai & Chiueh, 2006; Sanzi & Speidel, 2000), as summarized in the following:

- Two-dimensional batch interpolators (Hoeher et al., 1997);
- Successive one-dimensional batch interpolators (Hutter et al., 1999; Lai & Chiueh, 2006);
- Two-dimensional adaptive interpolators (Schafhuber & Matz, 2005; Schafhuber et al., 2003, April);
- Successive one-dimensional adaptive interpolators (Sanzi & Speidel, 2000).

Among the interpolation methods, Wiener filtering is a popular choice, since it can exploit the available information about the time-frequency correlation of the channel (Hoeher et al., 1997; Hutter et al., 1999; Sanzi & Speidel, 2000; Schafhuber & Matz, 2005; Schafhuber et al., 2003, April). A Wiener filter approach has been proposed also by Sgraja & Lindner (2003), without neglecting the ICI produced by the channel time variation within the OFDM block. Alternatively, an LS interpolation approach can be used, as done by Fertl & Matz (2006), who incorporated a trigonometric polynomial model of the time-frequency channel, and proposed a conjugate gradient algorithm with early termination to deal with the severe ill conditioning generated by fast LTV channels.

When the channel time variation is rapid, comb-type pilot placement schemes suffer from significant ICI. Besides zero-guarded pilots, another possible solution is to employ clustered pilot schemes, where groups of adjacent subcarriers are employed as pilots. This issue has been investigated in Shin, Andrews, & Powers (2007), where simulation results show that the MSE-optimal number of clusters is again equal to the number M of discrete-time channel paths. Moreover, as in the zero-guarded case, the M clusters should be equispaced.

7.3.2.3 *Data-Aided Channel Estimation and Tracking*

In the two previous subsections, we have considered the channel estimation task for two types of frequency-domain training: the zero-guarded clusters of Kannu & Schniter (2008), and the

classical (nonzero-guarded) comb pilot pattern used in DVB-T/H (ETSI, 2004). The first type, being MSE-optimal for CCE-BEM channels, obviously allows for good performance, at the price of a non-negligible rate reduction. On the other hand, focusing on a single OFDM block, the comb pattern of DVB-T/H minimizes the rate reduction due to training, at the price of a significant performance degradation caused by the unmodeled ICI. To overcome these drawbacks, a different type of training pattern should be adopted. Banelli, Cannizzaro, & Rugini (2007) used the zero-guarded clusters only for K_1 consecutive OFDM blocks, while no pilots are transmitted in the K_2 successive OFDM blocks. There are two key ideas in this approach. First, the time variability of the BEM coefficients over successive OFDM blocks is modeled as a first-order Gauss-Markov process, as expressed by

$$\mathbf{c}[k+1] = \tilde{\mathbf{A}}\mathbf{c}[k] + \boldsymbol{\nu}[k],$$

where $\tilde{\mathbf{A}}$ characterizes the BEM evolution and $\boldsymbol{\nu}[k]$ is the BEM innovation. This model permits LTV channel prediction from block to block during the K_2 blocks without pilots, by means of a Kalman filter (Banelli et al., 2007). Second, the same Kalman filter structure is exploited in a data-aided approach to refine the channel estimation over the K_2 blocks without pilots. Specifically, for each of the K_2 blocks, M equispaced data clusters are identified as virtual pilots, using a reliability-based selection metric. Using these virtual pilots, the BEM coefficients of the current block are iteratively estimated in a decision-directed mode, to obtain a better channel estimate and then more reliable data re-estimates. Successively, the BEM coefficients of the next block are predicted, and new virtual pilots are identified. For the virtual pilot selection, different reliability-based metrics are possible, based on the soft decisions and the MSE of the symbol estimates (Banelli et al., 2007).

The Kalman filter used by Banelli et al. (2007) is based on frequency-domain vector observations. To reduce complexity, a Kalman filter based on time-domain scalar observations can be employed (Muralidhar & Li, 2009). Indeed, the Kalman filter of Banelli et al. (2007) tracks a single vector that collects the BEM coefficients of all the paths, while the Kalman filter of Muralidhar & Li (2009) separately tracks each subvector related to the corresponding channel path, in a parallel way.

7.3.3 Iterative Channel Estimation and Turbo Equalization

Most of the ICI mitigation techniques investigated in the technical literature have two separate steps for channel estimation and channel equalization. However, joint channel estimation and equalization is a valid alternative, as shown by the data-aided approaches of Banelli et al. (2007) and Fang, Rugini, & Leus (2008, April). Additional performance improvement can be obtained by incorporating the channel decoder into the iterative scheme that performs joint channel estimation and ICI cancelation (Tomasin et al., 2005). In this section, we briefly describe the joint approach of Fang, Rugini, & Leus (2008, April), which combines the channel estimator of Tang et al. (2007) with the turbo equalizer of Fang et al. (2008). Specifically, the channel estimator can be modified in order to exploit the LLR values of the data produced by the turbo equalizer. These LLR values can be used to update the a priori symbol mean vector $\hat{\boldsymbol{\mu}}_a^{(\kappa)}[k]$, where κ is the iteration index. Since $\hat{\boldsymbol{\mu}}_a^{(\kappa)}[k]$ represents our current knowledge about the data vector $\mathbf{a}[k]$, an improved channel estimator can be designed by updating the model in (7.43), which becomes

$$\mathbf{y}_{\mathrm{W}}^{(\kappa)}[k] = \boldsymbol{\Omega}\big[\mathbf{I}_{MI} \otimes (\mathbf{p}[k] + \hat{\boldsymbol{\mu}}_a^{(\kappa)}[k])\big]\mathbf{c}[k] + \tilde{\mathbf{i}}_{\mathrm{W}}^{(\kappa)}[k] + \mathbf{z}_{\mathrm{W}}[k], \qquad (7.48)$$

where $\tilde{\mathbf{i}}_{W}^{(\kappa)}[k] \triangleq \mathbf{H}_{W}[k](\mathbf{a}[k] - \hat{\boldsymbol{\mu}}_{a}^{(\kappa)}[k])$ is the updated data-dependent interference. From (7.48), it is clear that $\mathbf{p}[k] + \hat{\boldsymbol{\mu}}_{a}^{(\kappa)}[k]$ can be considered as a new pilot vector, which incorporates our soft knowledge $\hat{\boldsymbol{\mu}}_{a}^{(\kappa)}[k]$ about the data $\mathbf{a}[k]$, while $\tilde{\mathbf{i}}_{W}^{(\kappa)}[k]$ represents the interference coming from the unknown part of the data. Since the interference power is reduced, the channel estimator exhibits improved performance, which helps the turbo equalizer to refine the estimate $\hat{\boldsymbol{\mu}}_{a}^{(\kappa)}[k]$ used at the next iteration. This iterative channel estimation and turbo equalization approach yields improved performance not only in the presence of zero-guarded pilot clusters but also when (nonzero-guarded) comb pilots are used as training pattern (Fang et al., 2008).

Alternatively, iterative channel estimation can be performed using both a time-domain preamble and (nonzero-guarded) frequency-domain pilots and exploiting the soft data outputs of the channel decoder (Zhao, Shi, & Reed, 2008). Specifically, the iterative channel estimator of Zhao et al. (2008) neglects the time variation of the channel within the OFDM block, and therefore, the ICI is considered as an additional noise.

7.3.4 Impact of Channel Estimation on BER Performance

The aim of this section is to understand how much performance loss is introduced by channel estimation errors at the receiver side. We consider an OFDM system with $L = 128$ subcarriers, of which $P = 21$ are dedicated to zero-guarded pilot symbols and $A = L - P = 107$ to QPSK data symbols. The $P = 21$ pilot symbols are divided into 7 clusters of length 3, i.e., each nonzero pilot is surrounded by a single zero on each side. The average pilot power of each cluster is equal to the data power. We consider a WSSUS Rayleigh fading channel with uniform delay power profile and channel length $M = 6$. The CP length is set to $L_{CP} = 5$. Regarding the time variation of the channel, we assume a Jakes' Doppler power profile with $\vartheta_{max} = 0.12$. The receiver window used for both channel estimation and equalization is MBAE-SOE with $D_b = 3$. Each channel path is modeled using a discrete Karhunen–Loève BEM with $I = 5$ basis functions. To estimate the LTV channel, all pilot and data locations are exploited, i.e., the number of observations is $\omega = L = 128$. The LMMSE channel estimator described by Tang et al. (2007) is employed in order to provide the CSI to the iterative banded block MMSE equalizer of Fang et al. (2008). For $E_s/N_0 > 25$ dB, Tikhonov regularization is adopted at the receiver. Figure 7.9 compares the BER performance of the turbo banded block MMSE equalizer (Fang et al., 2008) with perfect CSI and estimated CSI. The performance gap is moderate, and it is noteworthy that in both cases the BER curve does not evidence any error floor for $E_b/N_0 < 30$ dB.

7.3.5 Channel Estimation in MIMO-OFDM

Compared to single-antenna OFDM systems, channel estimation for MIMO-OFDM systems is more difficult for two reasons. First, since multiple channels have to be estimated, additional pilot symbols should be inserted with respect to the single-channel case. The second reason is the presence of IAI arising from multiple transmit antennas, which adds to the ICI. Similarly to the ICI mitigation issue, LTV channel estimation in MIMO-OFDM systems is quite recent, and relatively few techniques have been proposed so far. One of these techniques has been discussed in Section 4.5.3. Here, we briefly list the main features of other proposed schemes, which can be used for both spatial multiplexing and space-time-frequency coded OFDM.
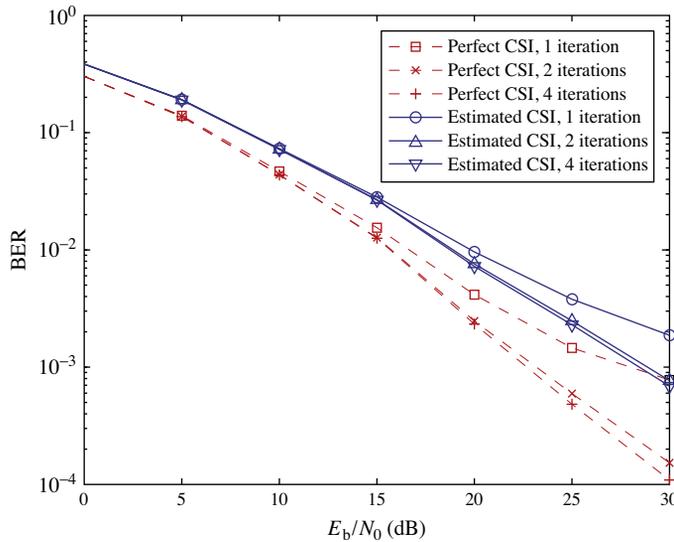
FIGURE 7.9

Effect of channel estimation on the BER performance.

Schafhuber, Rupp, Matz, & Hlawatsch (2003), have proposed a least-mean-squares-based adaptive approach to estimate a subsampled version of the MIMO frequency-domain channel matrix. The pilot symbols of each transmit antenna, which are orthogonal to those of the other antennas, are scattered comb-type nonzero-guarded pseudo-noise sequences. The optimum adaptation constants are obtained by automatic tuning (Schafhuber et al., 2003, June).

Salvo Rossi & Müller (2008) have used discrete prolate spheroidal sequences as basis functions to represent the MIMO channel transfer function. Pilot symbols are sparsely placed to sample the two-dimensional time-frequency channel. The linear MIMO channel estimators considered by Salvo Rossi & Müller (2008) counteract the IAI while ignoring the ICI.

Gao & Liu (2008) have proposed an expectation-maximization (EM) approach for maximum a posteriori (MAP) channel estimation. First, an LS estimator is designed for LTI channels, assuming the optimal pilot pattern presented by Barhumi, Leus, & Moonen (2003). Then, parallel ICI cancelation is included in the estimation process to deal with LTV channels. The proposed EM estimator also applies a low-rank approximation that avoids large matrix inversion, thereby reducing complexity.

Next, Li et al. (2008) have presented an LS estimator based on a linear model of the channel time variation. Orthogonal pilot clusters are assumed. The channel estimation task is performed before the data detection, neglecting the ICI coming from the data symbols.

Another MAP-based channel estimation scheme has been presented by Kim & Lim (2008). Also in this case, the ICI coming from the data symbols is neglected. A distinctive feature of the channel estimator of Kim & Lim (2008) is that $h^{(i,j)}[n,m]$ is obtained as a linear combination of the $\tilde{N}$ previous values $h^{(i,j)}[n-1,m],...,h^{(i,j)}[n-\tilde{N},m]$, where $\tilde{N} < L$, and i (j) is the index of the receive (transmit) antenna. In addition, to reduce the number of parameters, Kim & Lim (2008) assumes that

all the MM_TM_R MIMO channel paths have the same statistics and hence share the same set of linear combining coefficients.

Similarly to Zhao et al. (2008), the iterative channel estimator of Zhao, Shi, & Reed (2007) uses a time-domain preamble, frequency-domain pilots, and soft-decoded data. To deal with the MIMO scenario, space-time processing and IAI cancelation are included. Since the estimation process is carried out on a per-subcarrier basis, the estimation quality can be improved by a low-pass filter that exploits the frequency-domain channel correlation (Zhao et al., 2007).

7.4 CONCLUDING REMARKS

We now summarize some important issues about multicarrier systems transmitting over LTV channels. First, we stress that when the scattering function is separable, the ICI power only depends on the shape of the Doppler power profile and on the normalized maximum Doppler shift $\vartheta_{\max}$. On the other hand, the ICI power depends neither on the delay power profile of the channel (provided that the CP is sufficiently long) nor on the absolute maximum Doppler shift $\nu_{\max}$.

Second, we have shown that many options are available for channel estimation and ICI mitigation, with different performance levels and complexity requirements. In most cases, the use of statistical CSI (e.g., in window-aided receivers) guarantees a performance gain with negligible additional complexity. Therefore, statistical CSI should be exploited as much as possible. Note that the statistical CSI usually does not change as fast as the CIR.

Third, although we have focused on OFDM, most of the results discussed in this chapter can be extended to multiuser multicarrier systems, such as multicarrier CDMA (MC-CDMA) or orthogonal frequency-division multiple-access (OFDMA). For instance, one-tap MMSE equalizers and banded MMSE equalizers for MC-CDMA downlink systems have been investigated by Linnartz (2001) and by Rugini, Banelli, & Leus (2005, March), respectively, while an iterative joint channel estimator and multiuser detector for MC-CDMA uplink systems has been proposed by Zemen, Mecklenbräuker, Wehinger, & Müller (2006). Its extension for multiuser MIMO communications will be discussed in Chapter 8.

In the following, we highlight some topics related to OFDM system and application aspects, and then, we conclude this chapter by discussing some open issues.

7.4.1 System and Application Aspects

The first application aspect we consider is related to OFDM broadcasting systems designed as a single-frequency network (SFN). In a broadcasting SFN, many fixed transmitters (one for each geographical cell) transmit the same OFDM signal, using the same carrier frequency, so that a mobile receiver can avoid handovers. Therefore, the multiple signals are seen by the receiver as a single signal with different multipath components, which are beneficial from the frequency-diversity viewpoint. A drawback arises when two (or more) different multipath components have a significant relative delay so that the composite CIR seen by the receiver, i.e., the sum of the delayed CIRs, becomes very long. For instance, in DVB-T/H 8k, the length of a Typical Urban CIR is $M \approx 64$, while, due to the relative delays of the CIRs, the length of a composite CIR can be, e.g., $M_{\mathrm{comp}} \approx 750$. Here, the problem is not the CP length (assuming $L_{\mathrm{CP}} = L/8 = 1024$, the ISI is avoided), but the lack of enough DVB-T/H pilot symbols for

estimating the channel. Indeed, since the DVB-T/H pilot spacing is 12 times the subcarrier spacing, the maximum tolerated length of the composite CIR is $M_{max} \approx 8192/12 \approx 683$. Therefore, when a composite channel with CIR length $M_{comp} \approx 750$ is estimated using only the pilots of a single OFDM block, a delay-domain CIR aliasing arises, and the whole system performance degrades considerably. For LTI channels, this delay-domain aliasing is circumvented by exploiting the DVB-T/H scattered pilots of four OFDM blocks, thereby reducing the effective pilot spacing to $12/4 = 3$ and increasing M_{max} to $M_{max} \approx 8192/3 \approx 2971$, which is much greater than the limit given by the CP length $L_{CP} = 1024$. However, for fast LTV channels, the composite CIR changes from block to block, and therefore, the methods used for LTI channels are not appropriate.

Poggioni, Rugini, & Banelli (2009, June), avoided the delay-domain aliasing by means of an iterative algorithm that performs data-aided channel estimation. Basically, some data symbols are first estimated and successively used as virtual pilots to estimate the other data symbols. To reduce complexity, the positions of the virtual pilots are chosen to be equidistant from those of the pilot subcarriers. This way, the effective pilot spacing reduces to $12/2 = 6$ times the subcarrier spacing, and hence $M_{max} \approx 8192/6 \approx 1365$, which is beyond the CP limit $L_{CP} = 1024$. In the presence of a reduced number of pilots, other emerging techniques, such as compressed sensing, can also be employed to take advantage of the channel sparsity in the delay-Doppler domain (Tauböck, Hlawatsch, Eiwen, & Rauhut, 2010).

Another system aspect is the compatibility of the mentioned techniques with current OFDM standards, such as DVB-T/H. Clearly, the LTV equalization algorithms are fully compatible, since they only act at the receiver side. On the other extreme, pulse-shaping OFDM algorithms require a different transmitter and hence a moderate modification of current standards, due to the overlapping of different OFDM blocks. Besides, some channel estimation algorithms are not compatible, because they assume zero-guarded pilot patterns, differently from current standards. We identify three cases:

- Maximum compatibility: the receiver is designed assuming the current standard, at the price of a possibly low performance or a possibly high complexity;
- Moderate compatibility: the transmitter is slightly modified in order to simplify the receiver algorithms or to enhance the performance;
- No compatibility: in this case, an entirely new system design is performed, taking into account the requirements caused by fast LTV channels.

Multiuser systems can be specifically designed to deterministically reduce the ICI and the multiple-access interference (MAI): for instance, the multiuser multicarrier system of Leus, Zhou, & Giannakis (2003) completely removes both the ICI and the MAI for CCE-BEM channels, while an approximately MAI-free precoded multiuser OFDM system has been investigated by Tadjpour, Tsai, & Kuo (2007).

7.4.2 Open Issues

Even though OFDM systems with fast LTV channels have been largely investigated, there are still many questions that call for a definitive answer. One issue is related to the performance-complexity trade-off of structured equalizers, such as banded equalizers. Although the computational complexity of banded equalizers is well known, their theoretical performance has been scarcely investigated. A semianalytical approach that predicts the BER performance of banded linear block MMSE equalizers has been investigated by Rugini & Banelli (2007). However, little is known about the theoretical performance of nonlinear equalizers, such as ICI cancellers and turbo approaches. For instance, for DFEs,

only some performance bounds are available (Rugini & Banelli, 2007). Moreover, it is not completely clear which is the best structure (i.e., the best BEM basis) for channel estimation purposes. Simulation results of Tang et al. (2007) have shown that the polynomial BEM presents a reduced modeling error at low Doppler spread, while the modeling error of an oversampled complex exponential BEM and discrete Karhunen–Loève BEM is quite low at high Doppler spread. For BEMs based on statistical CSI, an aspect that deserves a deeper investigation is the robustness to mismatches of the Doppler power profile (Zemen & Mecklenbräuker, 2005). In addition, the BEM choice can affect both the equalization performance and the rate reduction caused by the number of pilots, as shown by Tang & Leus (2008) for CCE-BEM and polynomial BEM. Channel estimation by means of superimposed training is another interesting topic for further investigation (Zhang, Dai, Li, & Ye, 2009). In addition, it is still unknown whether it is advantageous to bypass the channel estimation step, for instance, by using noncoherent schemes (Hwang & Schniter, 2008; Wetz, Periša, Teich, & Lindner, 2008) (see also Section 6.4.5).

Undoubtedly, MIMO-OFDM systems present even more open issues than single-antenna OFDM systems. A significant issue is the pilot design (Dai, 2007), and the related channel estimation, which could exploit multiple OFDM blocks to reduce the pilot overhead, as done by Tang, Leus, & Banelli (2006) for single-antenna OFDM systems (see also Section 4.4). In addition, space-time-frequency codes could be specifically designed in order to counteract (or, better, to exploit) the rapid time variation of the channel. Last but not least, in MIMO-OFDM, time and frequency synchronization issues are important. In this case, synchronization algorithms should explicitly take into account the time variation of the channel, as done for single-antenna OFDM systems in Lv, Li, & Chen (2005), Mostofi & Cox (2007), Nguyen-Le & Le-Ngoc (2009) Lottici, Reggiannini, & Carta (2010).

References

Alamouti, S. M. (1998). A simple transmit diversity scheme for wireless communications. *IEEE Journal of Selected Areas in Communication*, *16*(10), 1415–1458.

Al-Gharabally, M., & Das, P. (2006, June). On the performance of OFDM systems in time varying channels with channel estimation error. In *Proceedings of the IEEE ICC-06*: (pp. 5180–5185). Istanbul, Turkey.

Amini, P., & Farhang-Boroujeny, B. (2009, June). Per-tone equalizer design and analysis of filtered multitone communication systems over time-varying frequency-selective channels. In *Proceedings of the IEEE ICC-09*, Dresden, Germany.

Armstrong, J. (1999). Analysis of new and existing methods of reducing intercarrier interference due to carrier frequency offset in OFDM. *IEEE Transactions on Communications*, *47*(3), 365–369.

Banelli, P., & Rugini, L. (2010, June). An H-infinity filtering approach for robust tracking of OFDM doubly-selective channels. In *Proceedings of the IEEE SPAWC-10*, Marrakech, Morocco.

Banelli, P., Cannizzaro, R. C., & Rugini, L. (2007, April). Data-aided Kalman tracking for channel estimation in Doppler-affected OFDM systems. In *Proceedings of the IEEE ICASSP-07*: Vol. 3, (pp. 133–136). Honolulu, HI.

Barbarossa, S., & Torti, R. (2001, May). Chirped-OFDM for transmissions over time-varying channels with linear delay/Doppler spreading. In *Proceedings of the IEEE ICASSP-01*: (pp. 2377–2380). Salt Lake City, UT.

Barhumi, I., Leus, G., & Moonen, M. (2003). Optimal training design for MIMO OFDM systems in mobile wireless channels. *IEEE Transactions on Signal Processing*, *51*(6), 1615–1624.

Barhumi, I., Leus, G., & Moonen, M. (2004). Time-domain and frequency-domain per-tone equalization for OFDM in doubly-selective channels. *Signal Processing*, *84*(11), 2055–2066.

Bello, P. A. (1963). Characterization of randomly time-variant linear channels. *IEEE Transactions on Communications Systems*, *11*(4), 360–393.

Bingham, J. A. C. (1990). Multicarrier modulation for data transmission: An idea whose time has come. *IEEE Communications Magazine*, *28*(5), 5–14.

Bölcskei, H. (2003). Orthogonal frequency division multiplexing based on offset QAM. In H. G. Feichtinger & T. Strohmer (Eds.), *Advances in Gabor analysis*, (pp. 321–352). Boston: Birkhäuser.

Borah, D. K., & Hart, B. D. (1999). Frequency-selective fading channel estimation with a polynomial time-varying channel model. *IEEE Transactions on Communications*, *47*(6), 862–873.

Cai, X., & Giannakis, G. B. (2003). Bounding performance and suppressing intercarrier interference in wireless mobile OFDM. *IEEE Transactions on Communications*, *51*(12), 2047–2056.

Cannizzaro, R. C., Banelli, P., & Leus, G. (2006, August). Adaptive channel estimation for OFDM systems with Doppler spread. In *Proceedings of the IEEE SPAWC-06*, Cannes, France.

Chang, K., Han, Y., Ha, J., & Kim, Y. (2006, May). Cancellation of ICI by Doppler effect in OFDM systems. In *Proceedings of the IEEE VTC-06 Spring*: (pp. 1411–1415). Melbourne, Australia.

Chen, S., & Yao, T. (2004). Intercarrier interference suppression and channel estimation for OFDM systems in time-varying frequency-selective fading channels. *IEEE Transactions on Consumer Electronics*, *50*(2), 429–435.

Chiavaccini, E., & Vitetta, G. M. (2000). Error performance of OFDM signaling over doubly-selective Rayleigh fading channels. *IEEE Communications Letters*, *4*(7), 328–330.

Choi, Y.-S., Voltz, P. J., & Cassara, F. A. (2001). On channel estimation and detection for multicarrier signals in fast and selective Rayleigh fading channels. *IEEE Transactions on Communications*, *49*(8), 1375–1387.

Chow, J., & Jeremic, D. (2006, November). Diversity benefits of OFDM in fast fading. In *Proceedings of the IEEE GLOBECOM-06*, San Francisco, CA.

Cimini, L. J., Jr. (1985). Analysis and simulation of a digital mobile channel using orthogonal frequency division multiplexing. *IEEE Transactions on Communications*, *33*(7), 665–675.

Cui, T., & Tellambura, C. (2007). Blind receiver design for OFDM systems over doubly-selective channels. *IEEE Transactions on Communications*, *55*(5), 906–917.

Dai, X. (2007). Optimal training design for linearly time-varying MIMO/OFDM channels modelled by a complex exponential basis expansion. *IET Communications*, *1*(5), 945–953.

Dao, D. N., & Tellambura, C. (2005). Intercarrier interference self-cancellation space-frequency codes for MIMO-OFDM. *IEEE Transactions on Vehicular Technology*, *54*(5), 1729–1738.

Das, S., & Schniter, P. (2007). Max-SINR ISI/ICI-shaping multicarrier communication over the doubly dispersive channel. *IEEE Transactions on Signal Processing*, *55*(12), 5782–5795.

Erseghe, T., Laurenti, N., & Cellini, V. (2005). A multicarrier architecture based upon the affine Fourier transform. *IEEE Transactions on Communications*, *53*(5), 853–862.

ETSI (2004, November). *Digital video broadcasting (DVB); framing structure, channel coding and modulation for digital terrestrial television.* EN 300 744, V1.5.1. Sophia Antipolis, France: European Telecommunications Standards Institute.

ETSI (2005, July). *Digital audio broadcasting (DAB); data broadcasting – MPEG-2 TS streaming.* TS 102 427, V1.1.1. Sophia Antipolis, France: European Telecommunications Standards Institute.

Fang, K., Leus, G., & Rugini, L. (2006, November-December). Alamouti space-time coded OFDM systems in time- and frequency-selective channels. In *Proceedings of the IEEE GLOBECOM-06*, San Francisco, CA.

Fang, K., Rugini, L., & Leus, G. (2008, April). Iterative channel estimation and turbo equalization for time-varying OFDM systems. In *Proceedings of the IEEE ICASSP-08*: (pp. 2909–2912). Las Vegas, NV.

Fang, K., Rugini, L., & Leus, G. (2008). Low-complexity block turbo equalization for OFDM systems in time-varying channels. *IEEE Transactions on Signal Processing*, *56*(11), 5555–5566.

Feng, S., Minn, H., Yan, L., & Jinhui, L. (2010). PIC-based iterative SDR detector for OFDM systems in doubly-selective fading channels. *IEEE Transactions on Wireless Communications*, *9*(1), 86–91.

Fertl, P., & Matz, G. (2006, October). Efficient OFDM channel estimation in mobile environments based on irregular sampling. In *Proceedings of the IEEE Asilomar-06*: (pp. 1777–1781). Pacific Grove, CA.

Fu, Y., Tellambura, C., & Krzymien, W. A. (2007). Transmitter precoding for ICI reduction in closed-loop MIMO OFDM systems. *IEEE Transactions on Vehicular Technology*, *56*(1), 115–125.

Gao, J., & Liu, H. (2008). Low-complexity MAP channel estimation for mobile MIMO-OFDM systems. *IEEE Transactions on Wireless Communications*, *7*(3), 774–780.

Gorokhov, A., & Linnartz, J.-P. (2004). Robust OFDM receivers for dispersive time-varying channels: Equalization and channel acquisition. *IEEE Transactions on Communications*, *52*(4), 572–583.

Gradshteyn, I. S., & Ryzhik, I. M. (1994). *Table of integrals, series, and products*. (5th ed.). Florida: Academic Press.

Haas, R., & Belfiore, J.-C. (1997). A time-frequency well-localized pulse for multiple carrier transmission. *Wireless Personal Communications*, *5*(1), 1–18.

Hampejs, M., Švač, P., Tauböck, G., Gröchenig, K., Hlawatsch, F., & Matz, G. (2009, June). Sequential LSQR-based ICI equalization and decision-feedback ISI cancellation in pulse-shaped multicarrier systems. In *Proceedings of the IEEE SPAWC-09*: (pp. 1–5). Perugia, Italy.

Harris, F. J. (1978, January). On the use of windows for harmonic analysis with the discrete Fourier transform. *Proceedings of the IEEE*, *66*(1), 51–83.

Hoeher, P., Kaiser, S., & Robertson, P. (1997, April). Two-dimensional pilot-symbol-aided channel estimation by Wiener filtering. In *Proceedings of the IEEE ICASSP-97*: (pp. 1845–1848). Munich, Germany.

How, W.-S., & Chen, B.-S. (2005). ICI cancellation for OFDM communication systems in time-varying multipath fading channels. *IEEE Transactions on Wireless Communications*, *4*(9), 2100–2110.

Hrycak, T., & Matz, G. (2006, October). Low-complexity time-domain ICI equalization for OFDM communications over rapidly varying channels. In *Proceedings of the IEEE Asilomar-06*: (pp. 1767–1771). Pacific Grove, CA.

Huang, D., Letaief, K. B., & Lu, J. (2005). Bit-interleaved time-frequency coded modulation for OFDM systems over time-varying channels. *IEEE Transactions on Communications*, *53*(7), 1191–1199.

Hunziker, T., & Dahlhaus, D. (2003). Iterative detection for multicarrier transmission employing time-frequency concentrated pulses. *IEEE Transactions on Communications*, *51*(4), 641–651.

Hutter, A. A., Hasholzner, R., & Hammerschmidt, J. S. (1999, September). Channel estimation for mobile OFDM systems. In *Proceedings of the IEEE VTC-99 Fall*: (pp. 305–309). Amsterdam, The Netherlands.

Hwang, S.-J., & Schniter, P. (2006). Efficient sequence detection of multi-carrier transmissions over doubly dispersive channels. *EURASIP Journal on Applied Signal Processing*, article ID 93638.

Hwang, S.-J., & Schniter, P. (2008). Efficient multicarrier communication for highly spread underwater acoustic channels. *IEEE Journal on Selected Areas in Communications*, *26*(9), 1674–1683.

IEEE (1999). *Part 11: Wireless LAN medium access control (MAC) and physical layer (PHY) specifications: High-speed physical layer in the 5 GHz band.* New York: Institute of Electrical and Electronics Engineers.

IEEE (2006). *Part 16: Air interface for fixed and mobile broadband wireless access systems.* New York: Institute of Electrical and Electronics Engineers.

Jeon, W. G., Chang, K. H., & Cho, Y. S. (1999). An equalization technique for orthogonal frequency-division multiplexing systems in time-variant multipath channels. *IEEE Transactions on Communications*, *47*(1), 27–32.

Jung, P., & Wunder, G. (2007). The WSSUS pulse design problem in multicarrier transmission. *IEEE Transactions on Communications*, *55*(10), 1918–1928.

Kannu, A. P., & Schniter, P. (2008). Design and analysis of MMSE pilot-aided cyclic-prefixed block transmission for doubly selective channels. *IEEE Transactions on Signal Processing*, *56*(3), 1148–1160.

Kay, S. M. (1993). *Fundamentals of statistical signal processing, Vol. I: Estimation Theory*. (1st ed.), Upper Saddle River, NJ, Prentice Hall.

Keller, T., & Hanzo, L. (2000). Adaptive multicarrier modulation: A convenient framework for time-frequency processing in wireless communications. *Proceedings of the IEEE*, *88*(5), 611–640.

Kim, J., Heath, R. W., Jr & Powers, E. J. (2005). Receiver designs for Alamouti coded OFDM systems in fast fading channels. *IEEE Transactions on Wireless Communications*, *4*(2), 550–559.

Kim, J.-G., & Lim, J.-T. (2008). MAP-based channel estimation for MIMO-OFDM over fast Rayleigh fading channels. *IEEE Transactions on Vehicular Technology*, *57*(3), 1963–1968.

Kim, K., & Park, H. (2006, May). A low complexity ICI cancellation method for high mobility OFDM systems. In *Proceedings of the IEEE VTC-06 Spring*: (pp. 2528–2532), Melbourne, Australia.

Kou, Y. J., Lu, W.-S., & Antoniou, A. (2005, August). An iterative intercarrier-interference reduction algorithm for OFDM systems. In *Proceedings of the IEEE PACRIM-05*: (pp. 538–541), Victoria, Canada.

Kozek, W., & Molisch, A. F. (1998). Nonorthogonal pulseshapes for multicarrier communications in doubly dispersive channels. *IEEE Journal on Selected Areas in Communications*, *16*(8), 1579–1589.

Lai, I-W., & Chiueh, T.-D. (2006, May). One-dimensional interpolation based channel estimation for mobile DVB-H reception. In *Proceedings of the IEEE ISCAS-06*: (pp. 5207–5210). Kos, Greece.

Le Floch, B., Alard, M., & Berrou, C. (1995). Coded orthogonal frequency division multiplex. *Proceedings of the IEEE*, *83*(6), 982–996.

Leung, E., & Ho, P. (1998, June). A successive interference cancellation scheme for an OFDM system. In *Proceedings of the IEEE ICC-98*: (pp. 375–379), Atlanta, GA.

Leus, G. (2004, September). On the estimation of rapidly time-varying channels. In *Proceedings of the EUSIPCO-04*. (pp. 2227–2230), Vienna, Austria.

Leus, G., Zhou, S., & Giannakis, G. B. (2003). Orthogonal multiple access over time- and frequency-selective channels. *IEEE Transactions on Information Theory*, *49*(8), 1942–1950.

Li, G., Yang, H., Cai, L., & Gui, L. (2003, October). A low-complexity equalization technique for OFDM system in time-variant multipath channels. In *Proceedings of the IEEE VTC-03 Fall*: (pp. 2466–2470), Orlando, FL.

Li, R., Li, Y., & Vucetic, B. (2008, March-April). Iterative receiver for MIMO-OFDM systems with joint ICI cancellation and channel estimation. In *Proceedings of the IEEE WCNC-08*: (pp. 7–12), Las Vegas, NV.

Li, Y., & Cimini, L. J., Jr. (2001). Bounds on the interchannel interference of OFDM in time-varying impairments. *IEEE Transactions on Communications*, *49*(3), 401–404.

Lin, D.-B., Chiang, P.-H., & Li, H.-J. (2005). Performance analysis of two-branch transmit diversity block-coded OFDM systems in time-varying multipath Rayleigh-fading channels. *IEEE Transactions on Vehicular Technology*, *54*(1), 136–148.

Linnartz, J.-P. M. G. (2001). Performance analysis of synchronous MC-CDMA in mobile Rayleigh channel with both delay and Doppler spreads. *IEEE Transactions on Vehicular Technology*, *50*(6), 1375–1387.

Liu, D. N., & Fitz, M. P. (2008, September). Turbo MIMO equalization and decoding in fast fading mobile coded OFDM. In *Proceedings of the 2008 Allerton Conference*: (pp. 977–982), Monticello, IL.

Liu, K., Kadous, T., & Sayeed, A. M. (2004). Orthogonal time-frequency signaling over doubly dispersive channels. *IEEE Transactions on Information Theory*, *50*(11), 2583–2603.

Lottici, V., Reggiannini, R., & Carta, M. (2010). Pilot-aided carrier frequency estimation for filter-bank multicarrier wireless communications on doubly-selective channels. *IEEE Transactions on Signal Processing*, *58*(5), 2783–2794.

Lu, S., Kalbasi, R., & Al-Dhahir, N. (2006, September). OFDM interference mitigation algorithms for doubly-selective channels. In *Proceedings of the IEEE VTC-06 Fall*, Montreal, Canada.

Lv, T., Li, H., & Chen, J. (2005). Joint estimation of symbol timing and carrier frequency offset of OFDM signals over fast time-varying multipath channels. *IEEE Transactions on Signal Processing*, *53*(12), 4526–4535.

Ma, X., Giannakis, G. B., & Ohno, S. (2003). Optimal training for block transmissions over doubly-selective wireless fading channels. *IEEE Transactions on Signal Processing*, *51*(5), 1351–1366.

Martone, M. (2001) A multicarrier system based on the fractional Fourier transform for time-frequency-selective channels. *IEEE Transactions on Communications*, *49*(6), 1011–1020.

Matz, G., Schafhuber, D., Gröchenig, K., Hartmann, M., & Hlawatsch, F. (2007). Analysis, optimization, and implementation of low-interference wireless multicarrier systems. *IEEE Transactions on Wireless Communications*, *6*(5), 1921–1931.

Molisch, A. F., Toeltsch, M., & Vermani, S. (2007). Iterative methods for cancellation of intercarrier interference in OFDM systems. *IEEE Transactions on Vehicular Technology*, *56*(4), 2158–2167.

Mostofi, Y., & Cox, D. C. (2005). ICI mitigation for pilot-aided OFDM mobile systems. *IEEE Transactions on Wireless Communications*, *4*(3), 765–774.

Mostofi, Y., & Cox, D. C. (2007). A robust timing synchronization design in OFDM systems – Part 2: High-mobility cases. *IEEE Transactions on Wireless Communications*, *6*(12), 4340–4348.

Muralidhar, K., & Li, K. H. (2009). A low-complexity Kalman approach for channel estimation in doubly-selective OFDM systems. *IEEE Signal Processing Letters*, *16*(7), 632–635.

Muschallik, C. (1996). Improving an OFDM reception using an adaptive Nyquist windowing. *IEEE Transactions on Consumer Electronics*, *42*(3), 259–269.

Nguyen-Le, H., & Le-Ngoc, T. (2009, June). Joint synchronization and channel estimation for OFDM transmissions over doubly selective channels. In *Proceedings of the IEEE ICC-09*, Dresden, Germany.

Ohno, S. (2005, March). Maximum likelihood inter-carrier interference suppression for wireless OFDM with null subcarriers. In *Proceedings of the IEEE ICASSP-05*, (pp. 849–852), Philadelphia, PA.

Ozdemir, M. K., & Arslan, H. (2007). Channel estimation for wireless OFDM systems. *IEEE Communications Surveys and Tutorials*, *9*(2), 18–48.

Park, K. W., & Cho, Y. S. (2005). An MIMO-OFDM technique for high-speed mobile channels. *IEEE Communications Letters*, *9*(7), 604–606.

Peiker, E., Dominicus, J., Teich, W., & Lindner, J. (2008, December). Improved performance of OFDM systems for fast time-varying channels. In *Proceedings of the IEEE ICSPCS-08*, Gold Coast, Australia.

Poggioni, M., Rugini, L., & Banelli, P. (2008). A novel simulation model for coded OFDM in Doppler scenarios. *IEEE Transactions on Vehicle Technology*, *57*(5), 2969–2980.

Poggioni, M., Rugini, L., & Banelli, P. (2009, June). Multistage decoding-aided channel estimation and equalization for DVB-H in single-frequency networks. In *Proceedings of the IEEE SPAWC-09*: (pp. 181–185), Perugia, Italy.

Poggioni, M., Rugini, L., & Banelli, P. (2009). DVB-T/H and T-DMB: Physical layer performance comparison in fast mobile channels. *IEEE Transactions on Broadcasting*, *55*(4), 719–730.

Robertson, P., & Kaiser, S. (1999, September). The effects of Doppler spreads in OFDM(A) mobile radio systems. In *Proceedings of the IEEE VTC-99 Fall*: (pp. 329–333), Amsterdam, The Netherlands.

Rugini, L., & Banelli, P. (2006, September). Banded equalizers for MIMO-OFDM in fast time-varying channels. In *Proceedings of the EUSIPCO-06*, Florence, Italy.

Rugini, L., & Banelli, P. (2007, June). Performance analysis of banded equalizers for OFDM systems in time-varying channels. In *Proceedings of the IEEE SPAWC-07*, Helsinki, Finland.

Rugini, L., Banelli, P., & Leus, G. (2005, March). Reduced-complexity equalization for MC-CDMA systems over time-varying channels. In *Proceedings of the IEEE ICASSP-05*, Vol. 3, (pp. 473–476), Philadelphia, PA.

Rugini, L., Banelli, P., & Leus, G. (2005). Simple equalization of time-varying channels for OFDM. *IEEE Communications Letters*, *9*(7), 619–621.

Rugini, L., Banelli, P., & Leus, G. (2006). Low-complexity banded equalizers for OFDM systems in Doppler spread channels. *EURASIP Journal on Applied Signal Processing*, article ID 67404, (pp. 13).

Rugini, L., Banelli, P., Fang, K., & Leus, G. (2009, June). Enhanced turbo MMSE equalization for MIMO-OFDM over rapidly time-varying frequency-selective channels. In *Proceedings of the IEEE SPAWC-09*: (pp. 36–40), Perugia, Italy.

Russell, M., & Stüber, G. L. (1995, July). Interchannel interference analysis of OFDM in a mobile environment. In *Proceedings of the IEEE VTC-95*: (pp. 820–824), Chicago, IL.

Salvo Rossi, P., & Müller, R. R. (2008). Slepian-based two-dimensional estimation of time-frequency variant MIMO-OFDM channels. *IEEE Signal Processing Letters*, *15*(1), 21–24.

Sanzi, F., & Speidel, J. (2000). An adaptive two-dimensional channel estimator for wireless OFDM with application to mobile DVB-T. *IEEE Transactions on Broadcasting*, *46*(2), 128–133.

Sari, H., Karam, G., & Jeanclaude, I. (1995). Transmission techniques for digital terrestrial TV broadcasting. *IEEE Communications Magazine*, *33*(2), 100–109.

Schafhuber, D., & Matz, G. (2005). MMSE and adaptive prediction of time-varying channels for OFDM systems. *IEEE Transactions on Wireless Communications*, *4*(2), 593–602.

Schafhuber, D., Matz, G., & Hlawatsch, F. (2003, April). Adaptive Wiener filters for time-varying channel estimation in wireless OFDM systems. In *Proceedings of the IEEE ICASSP-03*: (pp. 688–691), Hong Kong.

Schafhuber, D., Rupp, M., Matz, G., & Hlawatsch, F. (2003, June). Adaptive identification and tracking of doubly selective fading channels for wireless MIMO-OFDM systems. In *Proceedings of the IEEE SPAWC-03*: (pp. 417–421), Rome, Italy.

Schniter, P. (2004). Low-complexity equalization of OFDM in doubly selective channels. *IEEE Transactions on Signal Processing*, *52*(4), 1002–1011.

Seyedi, A., & Saulnier, G. J. (2005). General ICI self-cancellation scheme for OFDM systems. *IEEE Transactions on Vehicular Technology*, *54*(1), 198–210.

Sgraja, C., & Lindner, J. (2003, May). Estimation of rapid time-variant channels for OFDM using Wiener filtering. In *Proceedings of the IEEE ICC-03*: (pp. 2390–2395), Anchorage, AK.

Shin, C., Andrews, J. G., & Powers, E. J. (2007). An efficient design of doubly selective channel estimation for OFDM systems. *IEEE Transactions on Wireless Communications*, *6*(10), 3790–3802.

Song, H., Kim, J., Nam, S., Yu, T., & Hong, D. (2008). Joint Doppler-frequency diversity for OFDM systems using hybrid interference cancellation in time-varying multipath fading channels. *IEEE Transactions on Vehicular Technology*, *57*(1), 635–641.

Song, W. G., & Lim, J. T. (2006). Channel estimation and signal detection for MIMO-OFDM with time varying channels. *IEEE Communications Letters*, *10*(7), 540–542.

Stamoulis, A., Diggavi, S. N., & Al-Dhahir, N. (2002). Intercarrier interference in MIMO OFDM. *IEEE Transactions on Signal Processing*, *50*(10), 2451–2464.

Stantchev, B., & Fettweis, G. (2000). Time-variant distortions in OFDM. *IEEE Communications Letters*, *4*(9), 312–314.

Strohmer, T., & Beaver, S. (2003). Optimal OFDM design for time-frequency dispersive channels. *IEEE Transactions on Communications*, *51*(7), 1111–1122.

Tadjpour, L., Tsai, S. H., & Kuo, C. C. J. (2007). An approximately MAI-free multiaccess OFDM system in fast time-varying channels. *IEEE Transactions on Signal Processing*, *55*(7), 3787–3799.

Tan, P., & Beaulieu, N. C. (2004). Reduced ICI in OFDM systems using the "better than" raised-cosine pulse. *IEEE Communications Letters*, *8*(3), 135–137.

Tang, Z., & Leus, G. (2008). A novel receiver architecture for single-carrier transmission over time-varying channels. *IEEE Journal on Selected Areas in Communications*, *26*(2), 366–377.

Tang, Z., Leus, G., & Banelli, P. (2006, August). Pilot-assisted time-varying OFDM channel estimation based on multiple OFDM symbols. In *Proceedings of the IEEE SPAWC-06*, Cannes, France.

Tang, Z., Cannizzaro, R. C., Leus, G., & Banelli, P. (2007). Pilot-assisted time-varying channel estimation for OFDM systems. *IEEE Transactions on Signal Processing*, *55*(5), 2226–2238.

Tauböck, G., Hampejs, M., Matz, G., Hlawatsch, F., & Gröchenig, K. (2007, June). LSQR-based ICI equalization for multicarrier communications in strongly dispersive and highly mobile environments. In *Proceedings of the IEEE SPAWC-07*, Helsinki, Finland.

Tauböck, G., Hlawatsch, F., Eiwen, D., & Rauhut, H. (2010). Compressive estimation of doubly selective channels in multicarrier systems: Leakage effects and sparsity-enhancing processing. *IEEE Journal on Selected Topics in Signal Processing*, *4*(2), 255–271.

ten Brink, S. (2001). Convergence behavior of iteratively decoded parallel concatenated codes. *IEEE Transactions on Communications*, *49*(10), 1727–1737.

Teo, K. A. D., & Ohno, S. (2005, November/December). Optimal MMSE finite parameter model for doubly-selective channels. In *Proceedings of the IEEE GLOBECOM-05*: (pp. 3503–3507), St. Louis, MO.

Tomasin, S., Gorokhov, A., Yang, H., & Linnartz, J. P. (2005). Iterative interference cancellation and channel estimation for mobile OFDM. *IEEE Transactions on Wireless Communications*, *4*(1), 238–245.

Tonello, A. M., & Pecile, F. (2008). Analytical results about the robustness of FMT modulation with several prototype pulses in time-frequency selective fading channels. *IEEE Transactions on Wireless Communications*, *7*(5), 1634–1645.

Tong, L., Sadler, B. M., & Dong, M. (2004). Pilot-aided wireless transmissions: General model, design criteria, and signal processing. *IEEE Signal Processing Magazine*, *21*(6), 12–25.

Tran, X. N., & Fujino, T. (2005, December). Groupwise successive ICI cancellation for OFDM systems in time-varying channels. In *Proceedings of the IEEE ISSPIT-05*: (pp. 489–494), Athens, Greece.

Tsatsanis, M. K., & Giannakis, G. B. (1996). Modeling and equalization of rapidly fading channels. *International Journal of Adaptive Control and Signal Processing*, *10*(2/3), 159–176.

Vahlin, A., & Holte, N. (1995). Optimal finite duration pulses for OFDM. *IEEE Transactions on Communications*, *44*(1), 10–14.

Vogeler, S., Brötje, L., Klenner, P., Kühn, V., & Kammeyer, K. D. (2004, September). Intercarrier interference suppression for OFDM transmission at very high velocities. In *Proceedings of the International OFDM-Workshop*, Dresden, Germany.

Wang, T., Proakis, J. G., Masry, E., & Zeidler, J. R. (2006). Performance degradation of OFDM systems due to Doppler spreading. *IEEE Transactions on Wireless Communications*, *5*(6), 1422–1432.

Wang, T., Proakis, J. G., & Zeidler, J. R. (2007). Interference analysis of filtered multitone modulation over time-varying frequency-selective fading channels. *IEEE Transactions on Communications*, *55*(4), 717–727.

Wang, Z., & Giannakis, G. B. (2000). Wireless multicarrier communications: Where Fourier meets Shannon. *IEEE Signal Processing Magazine*, *17*(3), 29–48.

Wang, Z., & Giannakis, G. B. (2003). Complex-field coding for OFDM over fading wireless channels. *IEEE Transactions on Information Theory*, *49*(3), 707–720.

Wetz, M., Periša, I., Teich, W., & Lindner, J. (2008). Robust transmission over fast fading channels on the basis of OFDM-MFSK. *Wireless Personal Communications*, *47*(1), 113–123.

Yun, J. Y., Chung, S. Y., & Lee, Y. H. (2007). Design of ICI canceling codes for OFDM systems based on capacity maximization. *IEEE Signal Processing Letters*, *14*(3), 169–172.

Zhang, H., & Li, Y. (2003). Optimum frequency-domain partial response encoding in OFDM system. *IEEE Transactions on Communications*, *51*(7), 1064–1068.

Zhang, H., Dai, X., Li, D., & Ye, S. (2009). Linearly time-varying channel estimation and symbol detection for OFDMA uplink using superimposed training. *EURASIP Journal on Wireless Communications and Networking*, article ID 307375, (pp. 11).

Zhang, Y., & Liu, H. (2006). Frequency-domain correlative coding for MIMO-OFDM systems over fast fading channels. *IEEE Communications Letters*, *10*(5), 347–349.

Zhang, Y. H., Lu, W. S., & Gulliver, T. A. (2007, June). A successive intercarrier interference reduction algorithm for OFDM systems. In *Proceedings of the IEEE ICC-07*: (pp. 2936–2941), Glasgow, UK.

Zhao, Y., & Häggman, S. G. (2001). Intercarrier interference self-cancellation scheme for OFDM mobile communication systems. *IEEE Transactions on Communications*, *49*(7), 1185–1191.

Zhao, Y., Leclercq, J. D., & Häggman, S. G. (1998). Intercarrier interference compression in OFDM communication systems by using correlative coding. *IEEE Communications Letters*, *2*(8), 214–216.

Zemen, T., & Mecklenbräuker, C. F. (2005). Time-variant channel estimation using discrete prolate spheroidal sequences. *IEEE Transactions on Signal Processing*, *53*(9), 3597–3607.

Zemen, T., Mecklenbräuker, C. F., Wehinger, J., & Müller, R. R. (2006). Iterative joint time-variant channel estimation and multi-user detection for MC-CDMA. *IEEE Transactions on Wireless Communications*, *5*(6), 1469–1478.

Zhao, M., Shi, Z., & Reed, M. C. (2007, November). An iterative receiver with channel estimation for MIMO-OFDM over a time and frequency dispersive fading channel. In *Proceedings of the IEEE GLOBECOM-07*: (pp. 4155–4159), Washington, DC.

Zhao, M., Shi, Z., & Reed, M. C. (2008). Iterative turbo channel estimation for OFDM system over rapid dispersive fading channel. *IEEE Transactions on Wireless Communications*, *7*(8), 3174–3184.

Zhu, J., Wen, S., & Du, Q. (2008). Space-frequency-Doppler coded OFDM over the time-varying Doppler fading channels. *International Journal of Electronics and Communications, (AEÜ)*, *62*, 307–315.

Zou, W. Y., & Wu, Y. (1995). COFDM: An overview. *IEEE Transactions on Broadcasting*, *41*(1), 1–8.